Spatiotemporal variability of dissolved inorganic macronutrients along the northern Antarctic Peninsula

Thiago Monteiro[1,2,3*], Sian Henley[4], Ricardo César Gonçalves Pollery[5], Carlos Rafael Borges Mendes[2,6], Mauricio Mata[1,2], Virginia Maria Tavano[6], Carlos Alberto Eiras Garcia[1,2], and Rodrigo Kerr[1,2,3*]

[1]Programa de Pós-Graduação em Oceanologia, Instituto de Oceanografia, Universidade Federal do Rio Grande (FURG), Av. Itália km 8, Rio Grande, 96203-900, RS, Brazil.

[2]Laboratório de Estudos dos Oceanos e Clima, Instituto de Oceanografia, Universidade Federal do Rio Grande (FURG), Av. Itália km 8, Rio Grande, 96203-900, RS, Brazil.

[3]Brazilian Ocean Acidification Network (BrOA), Rio Grande, 96203-900, RS, Brazil.

[4]School of GeoSciences, University of Edinburgh, Edinburgh, EH9 3FE, United Kingdom.

[5]Unidade Multiusuário de Análises Ambientais, Centro de Ciências da Saúde, Universidade Federal do Rio de Janeiro (UFRJ), Cidade Universitária, 21941-902 Rio de Janeiro, Brazil.

[6]Laboratório de Fitoplâncton e Microorganismos Marinhos, Instituto de Oceanografia, Universidade Federal do Rio Grande (FURG), Av. Itália, km 8, Rio Grande, RS, Brazil.

*Corresponding authors

Thiago Monteiro

E-mail: thiagomonteiro@furg.br

Rodrigo Kerr

E-mail: rodrigokerr@furg.br

Highlights

- A novel macronutrients dataset is presented for the northern Antarctic Peninsula (NAP; 2003-2019).

- CDW is the main source of macronutrients, but local sources are also important in the region.

- Substantial interannual variability in macronutrients driven mainly by the water messes mixing, which is modulated by SAM and ENSO.

Abstract

The northern Antarctic Peninsula (NAP) is a key region of the Southern Ocean due to its complex ocean dynamics, distinct water mass sources, and the climate-driven changes taking place in the region. Despite the importance of macronu-

trients in fuelling primary production and driving the strong carbon uptake and storage, little is known about their spatiotemporal variability along the NAP. Hence, we explored a 24-year time series in this region, primarily sampled by the Brazilian High Latitude Group, to understand the processes involved in the spatial and interannual variability of macronutrients. We found high macronutrients concentrations, even in surface waters and under strong phytoplankton blooms. Minimum concentrations of dissolved inorganic nitrogen (16 mol kg^{-1}), phosphate (0.7 mol kg^{-1}), and silicic acid (40 mol kg^{-1}) along the NAP are higher than those recorded in surrounding regions. The main source of macronutrients is the intrusions of modified Circumpolar Deep Water (mCDW), and this is enhanced by local sources, such as organic matter remineralisation, water mass mixing, and mesoscale structures. However, we identified a depletion in silicic acid due to influence of Dense Shelf Water (DSW) from the Weddell Sea. Macronutrient concentrations shows substantial interannual variability driven by the balance between the intrusions of mCDW and advection of DSW, which is largely modulated by the Southern Annular Mode and to some extent by El Niño-Southern Oscillation. These findings are critical to improving our understanding of the natural variability of this Southern Ocean ecosystem and how it is responding to climate changes.

1. Introduction

The Southern Ocean plays a critical role in regulating the global climate (e.g., Henley et al., 2020). Although Southern Ocean surface waters cover less than 20% of the global ocean, they account for 40-50% of the total oceanic uptake of anthropogenic carbon from the atmosphere (Khatiwala et al., 2009, Landschützer, et al., 2015). Part of the carbon uptake in the Southern Ocean is driven by photosynthesis during the summer, which is fuelled by high concentrations of macronutrients, supporting ecosystem functioning and carbon storage (Henley et al., 2020). Nevertheless, the Southern Ocean is one of the regions that experiences pronounced changes in biogeochemical properties, altering the functioning of the entire ecosystem (Henley et al., 2020 and references therein). A key region for understanding biogeochemical changes in the Southern Ocean is the northern Antarctic Peninsula (NAP), which has experienced rapid changes in the coupled atmosphere-ocean-cryosphere system (e.g., Kerr et al., 2018a; Henley et al., 2019). For example, investigations over the last two decades have reported changes in wind patterns (Dinniman et al., 2012), land and sea ice cover (Shepherd et al., 2018), biological activity (Seyboth et al., 2016; Mendes et al., 2018) and the carbonate system (Kerr et al., 2018a; Monteiro et al., 2020; Orselli et al., 2022).

The micronutrient iron is an important fuel for photosynthesis and known to be limiting for primary production in vast areas of the Southern Ocean (de Baar et al., 1995; Henley et al., 2020). However, the regions around the NAP were shown to have sufficient iron supply to sustain high levels of phytoplankton production and biomass (Ardelan et al., 2010). Moreover, the NAP is an important region of the Southern Ocean because it is one of the regions most impacted by the

Antarctic Circumpolar Current (ACC), which carries the Circumpolar Deep Water (CDW). CDW is a relatively old water mass sourced from North Atlantic Deep Water (e.g., Ferreira & Kerr, 2017), so it is low in dissolved oxygen and rich in remineralised carbon and macronutrients (Prézelin et al., 2000, 2004; Dinniman et al., 2012; Hauri et al., 2015). Since the NAP is one of the Antarctic coastal regions most exposed to the ACC, it is constantly influenced by CDW intrusions (García et al., 2002; Barlett et al., 2018; Wang et al., 2022), altering the biogeochemical dynamics in this region (Meredith et al., 2017; Henley et al., 2019; Orselli et al., 2020). The CDW is a relatively warm water mass (>1 °C) that intrudes into the intermediate layers along the NAP (Prézelin et al, 2000; Couto et al., 2017; Venables et al., 2017). The physical properties of CDW change as it is mixed with cooler and less saline waters, forming the modified CDW (mCDW) in the shelf and coastal domain (Couto et al., 2017; Venables et al., 2017).

The NAP coastal region encompasses the Gerlache and Bransfield Straits, and the northwestern Weddell Sea continental shelf (Figure 1). At the southernmost part of the NAP, the Gerlache Strait is a relatively shallow region (depth ~ 800 m), with high concentrations of sea ice (Monteiro et al., 2020b; Parra et al., 2020; Su et al., 2022) and strongly impacted by meltwater from continental glaciers (Cook et al., 2016; Silva et al., 2020; Meredith et al., 2022). Despite covering a small area, Gerlache Strait acts as a stronger summer CO_2 sink than regions with wider areas, such as Bransfield Strait (Monteiro et al., 2020a). This strong CO_2 sink behaviour is driven mainly by high primary productivity (Monteiro et al., 2020b; Costa et al., 2020), which sustains a diverse and productive food web (Dalla Rosa et al., 2008; Nowacek et al., 2011; Mendes et al., 2018). Indeed, intense blooms of diatoms (Costa et al., 2020) and high densities of krill (Nowacek et al., 2011), penguins (Pitman & Durban, 2010) and whales (Secchi et al., 2011) are recorded in Gerlache Strait. Towards the north, the Bransfield Strait is a region with rapid and dynamic ocean circulation (Zhou et al., 2006; Dotto et al., 2016; Sangrà et al., 2017; van Caspel et al., 2018; Damini et al., 2022) and comprises the western, central, and eastern basins, separated by relatively shallow sills (Figure 1b). The western basin is the shallowest (~1000 m), followed by the central (~ 2000 m) and eastern (~ 2500 m) basins.

The NAP surface circulation (Figure 1 a) is characterised by local surface water and the mCDW, mainly coming from the Bellingshausen Sea (Zhou et al. 2002, 2006; Sangrà et al. 2017). These surface waters are advected from the Gerlache Strait to the eastern basin of Bransfield Strait by a relatively intense mesoscale baroclinic jet known as the Bransfield Current (Zhou et al. 2002, 2006; Savidge & Amft 2009). This current flows in a southwest-northeast direction along the shelf break of the South Shetland Islands (Sangrà et al. 2017). The waters advected by the Bransfield Current are relatively warm (~1.25^{o}C) and highly productive (Mendes et al. 2018, Costa et al. 2020, 2021), being able to transport phytoplanktonic biomass and zooplanktonic organisms along the NAP (Ferreira et al. 2020). The western basin of Bransfield Strait is strongly influenced by mCDW intrusions at intermediate levels (Barlett et al., 2018; Wang et al.,

2022), while the central and eastern deep basins are fuelled by Dense Shelf Water (DSW) from the Weddell Sea (Dotto et al., 2016; Damini et al., 2022; Wang et al., 2022). DSW refers to distinct shelf water varieties (i.e., High Salinity Shelf Water and Low Salinity Shelf Water; Damini et al., 2022; Wang et al., 2022) sourced in the northwestern continental shelves of the Weddell Sea (van Caspel et al., 2018; Wang et al., 2022), east of the Antarctic Peninsula (Figure 1). Unlike mCDW, DSW is recently ventilated under the shelf domain, therefore it is cold (< -1 ºC) and rich in dissolved oxygen (Dotto et al., 2016; Damini et al., 2022; Wang et al., 2022).

The DSW is advected into the NAP and retained in its most pure form mainly in the central basin of Bransfield Strait, where there is intense mixing with the mCDW at intermediate and upper levels, changing its physical and biogeochemical properties (Dotto et al., 2016; Damini et al., 2022; Wang et al., 2022). Hence, while mCDW is transported from the south (i.e., Gerlache Strait, western basin of Bransfield Strait) at intermediate layers along the NAP, the DSW is advected in deeper layers from the north (i.e., eastern basin of Bransfield Strait) (Moffat & Meredith, 2018; Wang et al., 2022). On interannual timescales, the strength of mCDW intrusion and DSW advection along the NAP is driven by regional modes of climate variability, such as the Southern Annular Mode (SAM) and the El Niño–Southern Oscillation (ENSO) (Barlett et al., 2018; Damini et al., 2022; Wang et al., 2022). During positive SAM and/or negative ENSO, mCDW intrusion is intensified, weakening the spreading of DSW along the NAP. Conversely, when SAM is negative and/or ENSO is positive, DSW advection is strengthened and can reach the Gerlache Strait (Wang et al., 2022). Indeed, the DSW in the Gerlache Strait has already been identified through thermohaline signals (Parra et al., 2020; Wang et al., 2022) and anthropogenic carbon concentrations (Kerr et al., 2018b; Lencina-Avila et al., 2018).

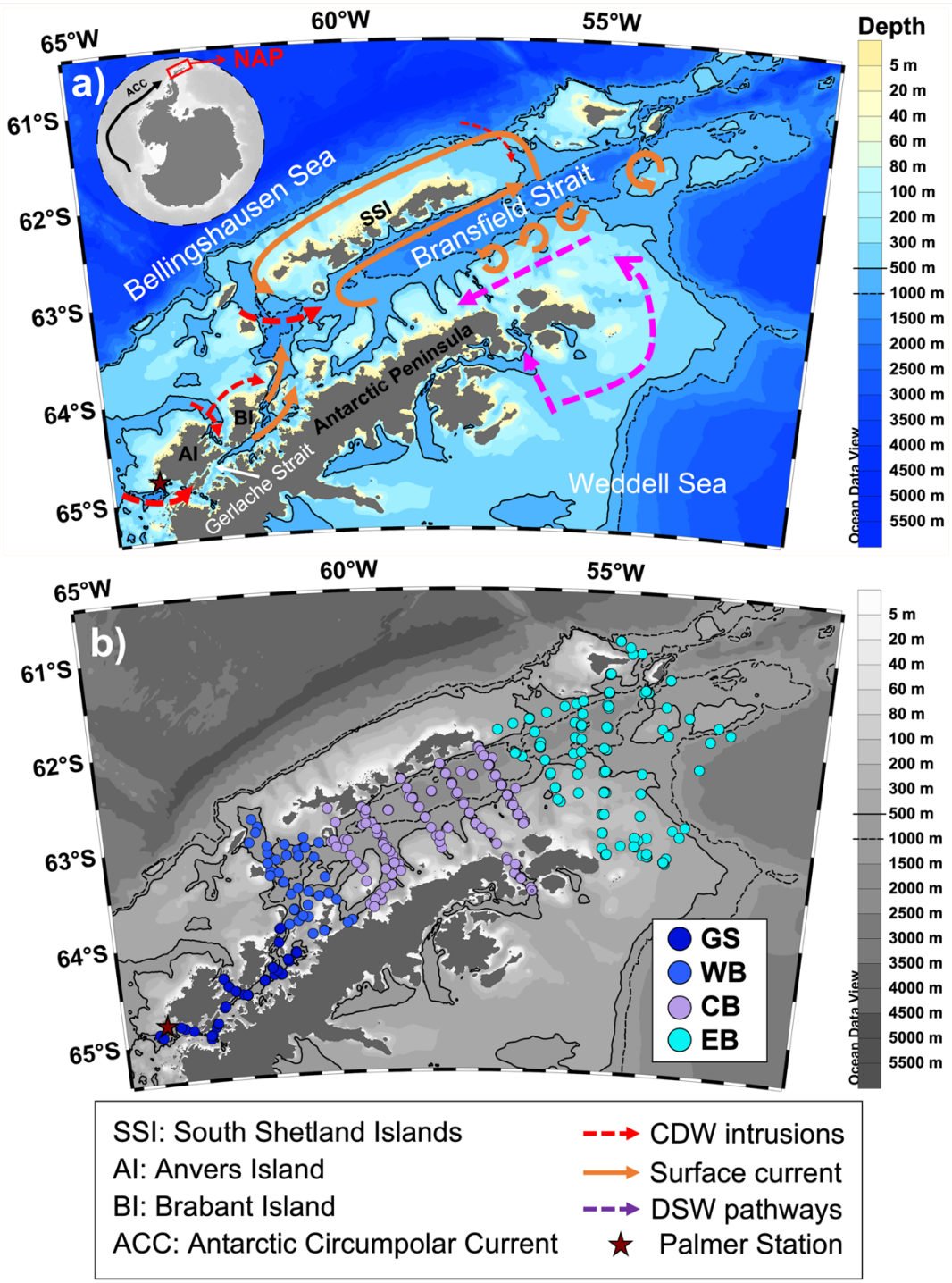
a)
b)
65°W
60°W
55°W
61°S
62°S
63°S
64°S
65°S
NAP
ACC
Bellingshausen Sea
SSI
Bransfield Strait
Antarctic Peninsula
BI
AI
Gerlache Strait
Weddell Sea
Depth
5 m
20 m
40 m
60 m
80 m
100 m
200 m
300 m
500 m
1000 m
1500 m
2000 m
2500 m
3000 m
3500 m
4000 m
4500 m
5000 m
5500 m
Ocean Data View
GS
WB
CB
EB
SSI: South Shetland Islands
AI: Anvers Island
BI: Brabant Island
ACC: Antarctic Circumpolar Current
CDW intrusions
Surface current
DSW pathways
Palmer Station

Figure 1: The northern Antarctic Peninsula (NAP) region and (a) ocean circulation pattern in the study area. The surface circulation (orange arrows), regions of mesoscale structures, as well as Circumpolar Deep Water (CDW) and Dense Shelf Water (DSW) pathways were based on previous studies (e.g., Wang et al., 2022; Dotto et al., 2016; Moffat & Meredith, 2018; Niiler et al., 1991; Sangrà et al., 2011, 2017; Savidge & Amft, 2009; Thompson et al., 2009; Zhou et al., 2002, 2006). The brown star in (a) and (b) depicts the U.S. Palmer Station location (64.8°S, 64.1°W), from which we extracted dissolved oxygen (Waite, 2022) used in figure 9 and macronutrients data (Ducklow et al., 2019) to validate the seasonal drawdown approach described in the methods. (b) Distribution of hydrographic stations where macronutrients were sampled and used in this study, including: Gerlache Strait (GS; purple dots), western (WB, red dots), central (CB, green dots), and eastern (EB, yellow dots) basins of the Bransfield Strait.

Furthermore, the environments along the NAP are influenced by mesoscale oceanographic processes that add complexity to the understanding of biogeochemistry in this region. The effect of shallow topography facilitates the upwelling of mCDW in Gerlache Strait and the western basin of Bransfield Strait (Venables et al., 2017; Parra et al., 2020), but little is known about its influence on macronutrient concentrations, which fuel primary production and enhance CO_2 uptake (Henley et al, 2019). The effect of topography and ocean circulation also leads to the formation of mesoscale eddies and increased eddy-fuelled productivity in the eastern basin of Bransfield Strait (Thompson & Heywood, 2009; Wang et al., 2022), although these processes are often neglected in biogeochemical studies due to their complexity (Jones et al., 2015). Understanding temporal variability patterns of macronutrients is also a challenge along the NAP, because the response time to SAM and ENSO variability modes is not well elucidated (Meredith et al., 2008; Barlett et al, 2018; Wang et al., 2022) and the mesoscale processes themselves may also play an important role in this variability (Meredith et al., 2017; Kerr et al., 2018a; Henley et al., 2019). For example, intense diatom blooms enhance CO_2 uptake (Brown et al., 2019; Costa et al., 2020) and can lead to nutrient depletion in the upper ocean and increase further local remineralisation of carbon and macronutrients below the mixed layer (Henley et al., 2017, 2018). In addition, melting sea and glacial ice regulates summer water column stability (Höfer et al., 2019; Wang et al., 2020), driving phytoplankton blooms (Kim et al., 2016; Brown et al., 2019; Costa et al., 2020), CO_2 uptake (Brown et al., 2019; Costa et al., 2020, Monteiro et al., 2020b), and nutrient depletion and replenishment in the upper ocean (Henley et al., 2017, 2018).

The importance of nutrients to fuel the primary production that underpins the food chain has been emphasised in some studies throughout the NAP (Mendes et al., 2018; Höfer et al., 2019; Costa et al., 2020; Mascioni et al., 2021), as well as the impact of mesoscale processes on nutrient supply (Wang et al., 2020; Forsch et al., 2021; Meredith et al., 2022). Furthermore, some studies have provided important information on the processes that regulate macronutrient concentrations south of the NAP, i.e., on the continental shelf of the Western

Antarctic Peninsula (WAP; Henley et al., 2019 and references therein), although little is known about these processes and their interannual variability in the NAP. Even less is known about the processes that regulate the spatial and temporal variability of macronutrients along the NAP and how the high complexity of this region is reflected in macronutrient concentrations. Therefore, we explored a dataset comprising 24 years of sampling to understand the processes involved in the spatial and temporal variability of macronutrients during the austral summer along the NAP.

2. Material and Methods

2.1 The hydrographic and macronutrient datasets

We compiled a time series spanning the period from 1996 to 2019 (Figures S1-S4) of the seawater hydrographic variables conservative temperature (°C), absolute salinity (g kg^{-1}) and dissolved oxygen (mol kg^{-1}), and the macronutrients nitrate, nitrite, ammonium, phosphate, and silicic acid (mol kg^{-1}). The study area covered the NAP regions including the Gerlache Strait, which separates the Anvers and Brabant Islands from the Antarctic Peninsula, and the Bransfield Strait, between the South Shetland Islands and the Peninsula (Figure 1a). To better understand the different processes influencing the variability of macronutrient concentrations, the sampling stations were split into four sub-regions: the Gerlache Strait and the western, central, and eastern basins of Bransfield Strait (Figure 1b). Most data (~90%) were obtained from the Brazilian High Latitude Oceanography Group (GOAL, Mata et al., 2018; Dotto et al., 2021) from austral summer field campaigns (January-March). In some years (1996, 2005, 2006, 2010, 2011) we used hydrographic and macronutrient data from GLODAP 2020 (Olsen et al., 2020) along the NAP and exceptionally for 1996 we used data available from December 1995 to February 1996 (the FRUELA cruises, García et al., 2022; Álvarez et al., 2002). Details on the sampling and analysis of macronutrient data obtained from GLODAP dataset can be accessed on the OCADS platform (https://www.ncei.noaa.gov/access/ocean-carbon-acidification-data-system-portal/).

2.2 Sampling and macronutrient analyses from GOAL dataset

For the GOAL dataset, hydrographic data profiles were measured, and discrete seawater samples were collected using a combined Sea-Bird CTD/Carousel 911 + system® equipped with oxygen sensors and 24 12 L Niskin bottles. Seawater samples were filtered through cellulose acetate membrane filters (0.45 µm) for determination of dissolved inorganic macronutrient concentrations (i.e., dissolved inorganic nitrogen (DIN): nitrate, nitrite, and ammonium; phosphate and silicic acid). Prior to 2015, the analyses were carried out on board immediately after collection and from 2015 onwards the samples were frozen immediately at −80°C until laboratory analysis. In both cases the analyses followed the spectrophotometric determination methods described by Aminot and Chaussepied (1983) with an accuracy around ± 5% for all analysed macronutrients. Orthophosphate was measured by reaction with ammonium molybdate, with ab-

sorption readings at 885 nm. Silicic acid measurements, in the form of reactive Si, were corrected for sea salt interference. Detection limits were 0.11 mol kg^{-1} for DIN, 0.10 mol kg^{-1} for phosphate and 0.50 mol kg^{-1} for silicic acid.

2.3 Summer average profiles of hydrographic properties and macronutrients

About 97% of the DIN data were composed of nitrate, followed by ammonium (2%) and nitrite (1%). Therefore, in some cases (11% of all data), we considered DIN as the nitrate concentration, when no nitrite and/or ammonium data were available. Discrete seawater samples were collected at irregular depth intervals from surface (5 m) to deep waters (at approximately 15 m from the bottom). We averaged the parameters for each region at regular depth intervals from the surface to the bottom (i.e., 0, 25, 50, 75, 100, 250, 500, 750, 1000, 1250, 1500, 1750, 2000 m) to obtain an averaged summer profile for each year (Figures S1-S4). All hydrographic and macronutrients data are freely available at https://doi.org/10.5281/zenodo.7384423 (Monteiro et al., 2022).

2.4 Seasonal macronutrient drawdown

We estimated seasonal macronutrient drawdown on the averaged profiles for each year (grey profiles in Figure 5) as the difference between the depth-integrated nutrient concentration between 50 and 100 m and the depth-integrated concentration between 0 and 50 meters. Therefore, we assumed that summer macronutrient concentrations between 50 and 100 m were representative of macronutrient concentrations between 0 and 50 m in the previous winter. Using this method, we also estimated the seasonal macronutrient drawdown on the averaged profiles for each year in the Palmer Station LTER data (Figure 1, Ducklow et al., 2019), where Kim et al. (2016) measured seasonal macronutrient drawdown from *in situ* data collected in winter and the following summer. Our estimates of seasonal macronutrient drawdown agree with the results obtained by Kim et al. (2016), which attests to the robustness of our adopted method based on summer data alone. They measured a seasonal drawdown from 1993 to 2013 of 415 ± 110 mmol m^{-2}, 23 ± 10 mmol m^{-2}, and 985 ± 386 mmol m^{-2} for DIN, phosphate, and silicic acid, respectively. For the same period, we estimated a seasonal drawdown of 411 ± 191 mmol m^{-2}, 25 ± 9 mmol m^{-2}, and 950 ± 269 mmol m^{-2} for DIN, phosphate, and silicic acid, respectively.

2.5 Composite macronutrient profiles by climate modes

To assess the influence of the SAM and ENSO modes of climate variability on the concentrations of macronutrients, we separated the austral summer profiles between years of positive and negative SAM or ENSO and calculated the difference between them. SAM index was obtained from the British Antarctic Survey website (http://www.nerc-bas.ac.uk/icd/gjma/sam.html), which is based on the differences between normalised monthly zonal means of sea-level pressure observations at 40°S and 65°S (Marshall, 2003). ENSO index was obtained from the Climate Prediction Centre (http://www.cpc.ncep.noaa.gov), which is defined as the consecutive three-month average of sea surface temperature anomalies from the ERSST.v4 dataset in the Niño 3.4 region (5°N – 5°S, 120°W

– 170°W; Vera and Osman 2018; La et al. 2019). Although the response time of physical and biogeochemical properties to variations in SAM and ENSO along the NAP is not well understood, it has been estimated to range from 4 to 6 months for SAM and 6 to 9 months for ENSO (e.g., Kim et al., 2016; Dotto et al., 2016; Meredith et al., 2008; Barllet et al., 2018). Here, we used a lag of 4 months from the sampling month for the SAM index and of 6 months for the ENSO index (Table S1).

We calculated the uncertainty propagated in calculating the difference between the averages through the following equation: $_z=\sqrt{(\ _{\bar{x}})^2 + (\ _{\bar{y}})^2}$, where "$\ _{\bar{x}}$" and "$\ _{\bar{y}}$" are the standard errors of each average. To assess the statistical difference between the average positive and negative SAM or ENSO profiles, we used Student's t-tests for normally distributed profiles. For profiles with non-normal distribution, we used the non-parametric Mann-Whitney-Wilcoxon test. To test the normal distribution, we used the Shapiro-Wilk statistical test.

3. Results

3.1 Spatial distribution of hydrographic properties and macronutrients along the northern Antarctic Peninsula

In general, the surface temperature was higher than 0°C along the NAP (Figure 2a). However, along the Bransfield Strait we observed a front between waters colder than 0°C towards the Antarctic Peninsula and waters warmer than 0°C towards the South Shetland Islands (Figure S5). Through the water column, the temperature was higher than 0°C at Gerlache Strait, decreasing (< 0°C) along the Bransfield Strait (Figure 2a). Temperatures higher than 0°C were observed at the southern end of Gerlache Strait and western basin of Bransfield Strait from the surface to the deep layer (Figure S5). Temperatures lower than –1°C were observed in the central basin of Bransfield Strait below 500 m and a slight temperature rise was observed at the eastern end of Bransfield Strait below 500m. Salinity was lower above 50 m (34.28 ± 0.18 g kg^{-1}) along the NAP (Figure 2b), and even lower in Gerlache Strait (34.09 ± 0.25 g kg^{-1}) (Figure S5). Below 200 m the salinity was relatively homogeneous in the central basin of Bransfield Strait (34.70 ± 0.04 g kg^{-1}), while there was an increase in salinity in the western basin of Bransfield Strait (34.72 ± 0.02 g kg^{-1}) and in the Gerlache Strait (34.79 ± 0.05 g kg^{-1}) (Figure 2b). Dissolved oxygen concentrations were lowest (< 225 µmol kg^{-1}) below the surface in the Gerlache Strait and western basin of Bransfield Strait, and highest (> 275 µmol kg^{-1}) in the central basin of Bransfield Strait, mainly below 1000 m (Figure 2c). The highest concentrations of DIN (> 35.00 µmol kg^{-1}) were observed in the transition between the central and eastern basins of Bransfield Strait below 500 m (Figure 2d). Although the DIN concentrations did not have as clear a west-east pattern as the other macronutrients, in general a slight increase in DIN concentration was observed in the central basin of Bransfield Strait. Average DIN concentration through the water column was 29.67 ± 3.09 µmol kg^{-1} in the Gerlache Strait and 28.23 ± 2.84 µmol kg^{-1}, 30.39 ± 2.49 µmol kg^{-1}, and 29.42 ± 2.08 µmol kg^{-1} in the

western, central, and eastern basins of Bransfield Strait, respectively.

Both phosphate (Figure 2e) and silicic acid (Figure 2f) concentrations were higher in the Gerlache Strait and western basin of Bransfield Strait than the rest of the NAP below the subsurface (50 m) down to 750 m. Average silicic acid concentration through the water column was 80.67 ± 8.99 µmol kg^{-1} in the Gerlache Strait and 74.71 ± 6.02 µmol kg^{-1}, 60.93 ± 4.72 µmol kg^{-1}, and 62.38 ± 7.87 µmol kg^{-1} in the western, central, and eastern basins of Bransfield Strait, respectively. Average phosphate concentration through the water column was 1.88 ± 0.26 µmol kg^{-1} in the Gerlache Strait and 2.00 ± 0.19 µmol kg^{-1}, 1.86 ± 0.20 µmol kg^{-1}, and 1.88 ± 0.17 µmol kg^{-1} in the western, central, and eastern basins of Bransfield Strait, respectively. We also observed high phosphate concentrations in both central (2.00 ± 0.21 µmol kg^{-1}) and eastern (1.99 ± 0.15 µmol kg^{-1}) basins of Bransfield Strait below 1000 m (Figure 2e). In some profiles in central and eastern basins of Bransfield Strait there were concentrations of phosphate (1.75 µmol kg^{-1}) and silicic acid (55.00 µmol kg^{-1}) in the deep layer as low as in the surface layer (Figure 2e,f). The lowest concentrations of silicic acid were recorded in the central basin of Bransfield Strait, from the surface to the deep layer (Figure S5).

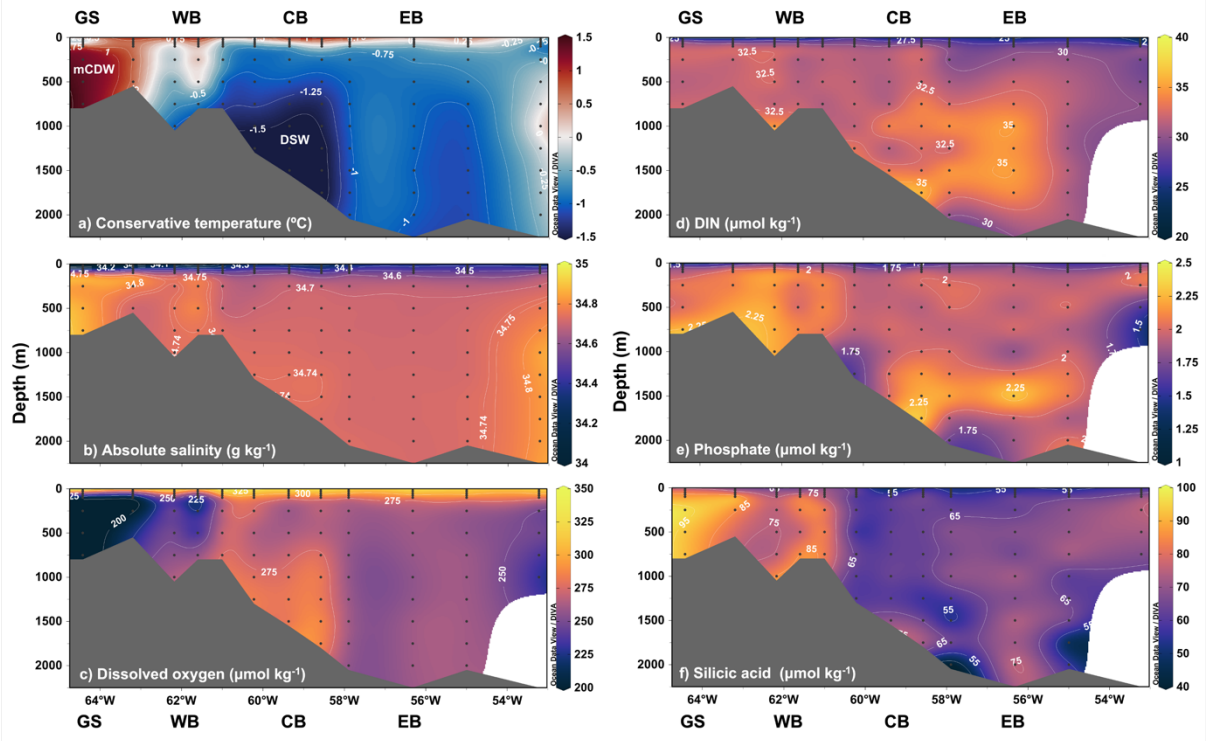

Figure 2: Zonal sections of water column distributions of (a) conservative temperature, (b) absolute salinity, (c) dissolved oxygen, (d) dissolved inorganic

nitrogen (DIN), (e) phosphate, and (f) silicic acid during austral summer (Jan-Mar) along the northern Antarctic Peninsula (NAP). Each profile composing the section are averaged profiles at each degree of longitude, considering the entire dataset (from 1996 to 2019). The zonal section comprises the regions from the south to north of the NAP: Gerlache Strait (GS), and the western (WB), central (CB) and eastern (EB) basins of Bransfield Strait. At the western end of the NAP (GS) there are intense intrusions of modified Circumpolar Deep Water (mCDW) whereas in the CB there are intense intrusions of Dense Shelf Water (DSW) from the Weddell Sea. Sampling depths are shown as grey dots.

The lowest temperatures ($< -1^{o}$C) below 500 m were associated with a greater influence of DSW while the highest temperatures ($> 0^{o}$C) were associated with a greater influence of mCDW in intermediate layers (Figure 3a). Lower dissolved oxygen concentrations (< 225 µmol kg^{-1}) were evident in warmer waters associated with the mCDW in contrast to the more oxygenated (> 275 µmol kg^{-1}) waters associated with DSW (Figure 3b). In general, the highest concentrations of phosphate (> 2 µmol kg^{-1}) and silicic acid (> 80 µmol kg^{-1}) were associated with greater influence of mCDW (Figure 3c-e) in intermediate and deep layers (Figure 3a), although high concentrations of DIN (> 30 µmol kg^{-1}) and phosphate (> 2 µmol kg^{-1}) were observed under the influence of DSW (Figure 3c-d). The lowest silicic acid concentrations below 500 m were observed under the influence of DSW, with concentrations (< 60 µmol kg^{-1}) as low as in the surface layer. However, silicic acid concentrations were also relatively high in the surface layer, reaching values > 70 µmol kg^{-1} (Figure 3c).

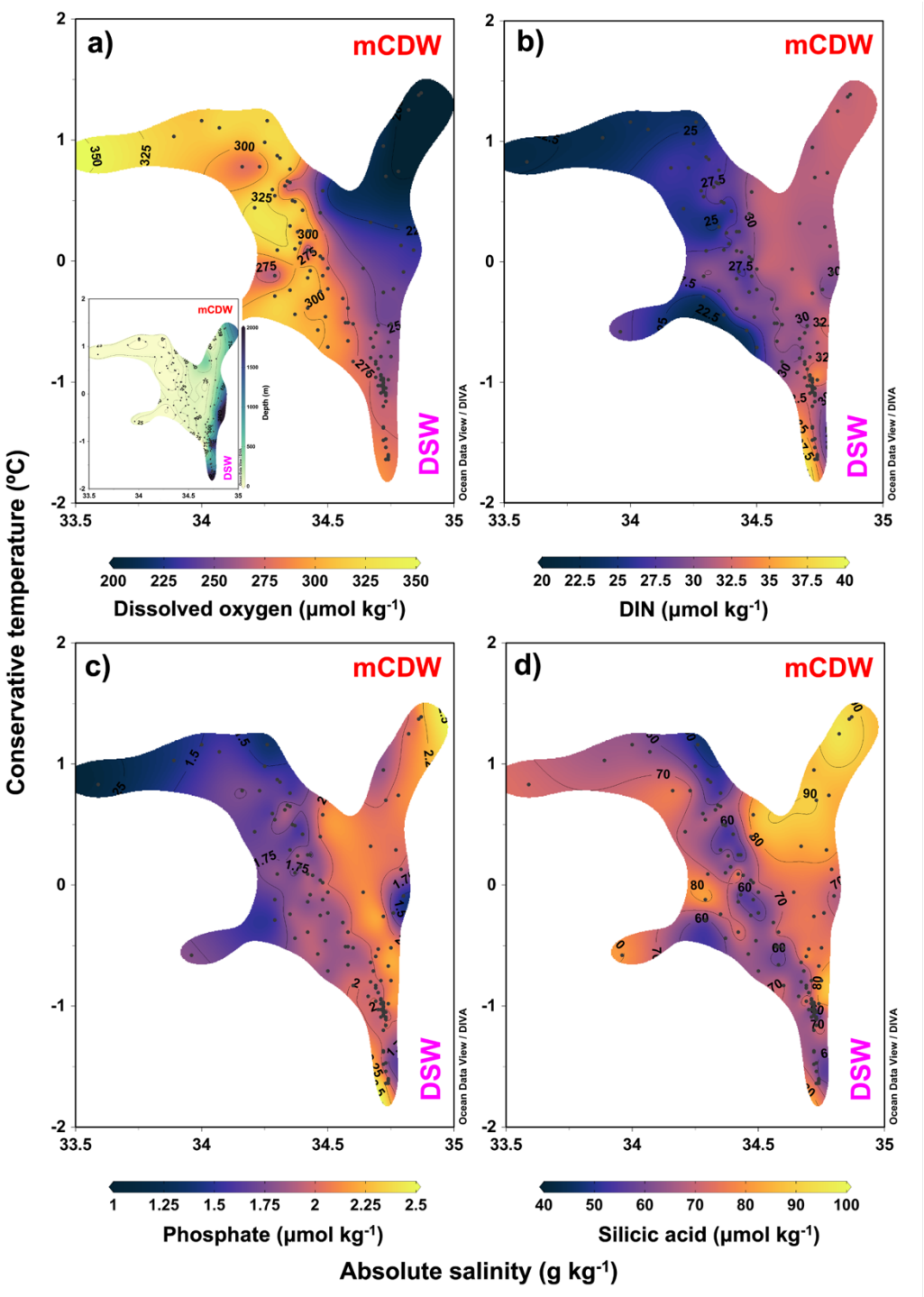
a)
mCDW
DSW
b)
mCDW
DSW
c)
mCDW
DSW
d)
mCDW
DSW
Ocean Data View / DIVA
Conservative temperature (ºC)
Absolute salinity (g kg-1)
Dissolved oxygen (µmol kg-1)
DIN (µmol kg-1)
Phosphate (µmol kg-1)
Silicic acid (µmol kg-1)
Depth (m)

Figure 3: Conservative temperature-absolute salinity (Θ-S_A) diagram vs properties during austral summer (Jan-Mar) along the northern Antarctic Peninsula. Θ-S_A vs (a) dissolved oxygen, (b) dissolved inorganic nitrogen (DIN), (c) phosphate, (d) silicic acid, and depth on the inset (a). In each Θ-S_A diagram the influence of mixing of modified Circumpolar Deep Water (mCDW) and Dense Shelf Water (DSW) is shown.

3.2 Interannual variability of hydrographic properties and macronutrients along the northern Antarctic Peninsula

The highest interannual variability in temperature was observed in the western basin of Bransfield Strait (Figure 4d), also associated with the highest variability of both salinity (Figure 4e) and dissolved oxygen, mainly in the depth interval 250-500m (Figure 4f) in the same area. Dissolved oxygen concentrations also showed interannual variability in the central (Figure 4i) and eastern (Figure 4l) basins of Bransfield Strait, albeit to a lesser degree and more homogeneously with depth. In the western basin of Bransfield Strait, there was an increase of more than 1°C between 250 m and 500 m with a subsequent decrease in the deep layer (Figure 4d) in 2008, when the highest salinities (Figure 4e) and the lowest concentrations of dissolved oxygen (Figure 4f) were also observed. Conversely, in the western and eastern basins of Bransfield Strait the temperature was anomalously lower than –1°C below 500 m in 2016, when the highest concentrations of dissolved oxygen (> 270 µmol kg^{-1}) below 250 m in the western basin of Bransfield Strait was also observed (Figure 4f). Gerlache Strait showed the second highest interannual variability in temperature and salinity among the regions examined here (Figure 4b,c). Even in the eastern basin of Bransfield Strait, with less temperature variability, there were variations of up to 1ºC among the years, but more homogeneously with depth (Figure 4j) than in the western basin of Bransfield Strait and Gerlache Strait. Other anomalous behaviours were recorded, such as the lowest concentration of dissolved oxygen in 2004 in Gerlache Strait (Figure 4c) and central basin of Bransfield Strait (Figure 4i), and in 2015 in the central (Figure 4i) and eastern (Figure 4l) basins of Bransfield Strait at 250 m. On the other hand, the highest anomalous concentrations of dissolved oxygen in central (Figure 4i) and eastern (Figure 4l) basins of Bransfield Strait were recorded in 2011.

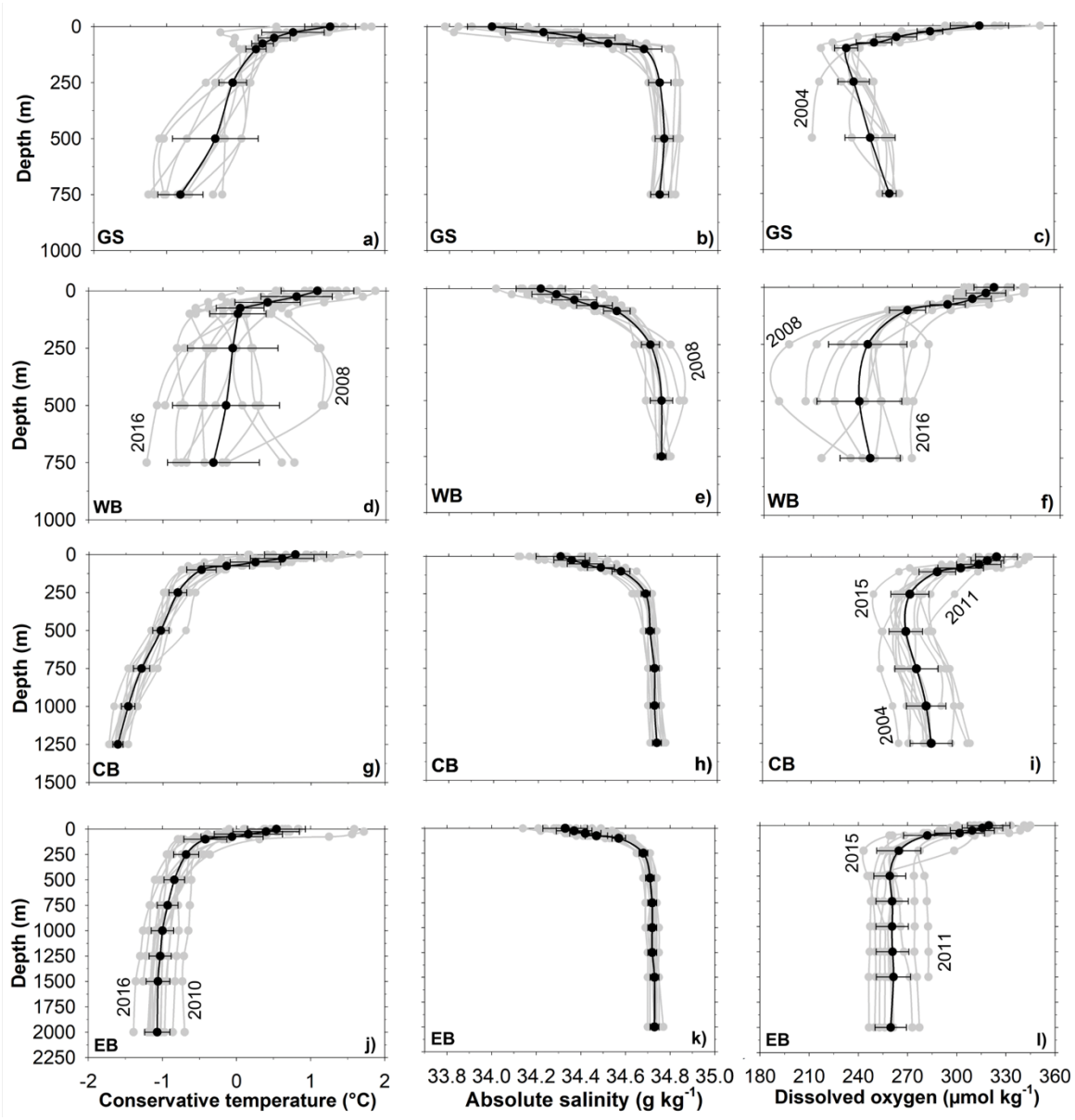

Figure 4: Summer (Jan-Mar) average profiles of hydrographic properties for each year from 1996 to 2019 along the northern Antarctic Peninsula, comprising the regions: (a-c) Gerlache Strait (GS), (d-f) western (WB), (g-i) central (CB), and (j-l) eastern (EB) basins of Bransfield Strait. Profiles for each year are presented in grey lines and the black lines are the averaged profiles over the period for each property and region. The horizontal black bars are the standard deviations for each depth. Years showing anomalous behaviour (i.e., outside the

standard deviation) are highlighted.

There was high interannual variability in the summer average profiles of all macronutrients along the NAP (Figure 5). The highest interannual variability was observed in silicic acid, with concentrations varying by up to a factor of three (~ 40-120 µmol kg^{-1}) through the water column (third column in Figure 5). In most profiles, the concentration of silicic acid increased from surface waters to ~100-200 m and then became more homogeneous with depth. DIN (first column in Figure 5) and phosphate (second column in Figure 5) concentrations were lower at the surface and consistently higher below 100 m. On average, silicic acid concentrations were highest in the western basin of Bransfield Strait (Figure 5f) and in Gerlache Strait, where the highest concentrations occurred in 2016 and 2017 (Figure 5c). The highest silicic acid concentrations were observed in 2017 and the lowest in 2014 along the entire NAP. However, silicic acid in 2017 were even higher, and throughout the entire water column, in the central and eastern basins of Bransfield Strait (Figure 5i,l) than in the western basin of Bransfield Strait and the Gerlache Strait (Figure 5c,f), where this increase was more pronounced below 100 m. In the central basin of Bransfield Strait there was higher interannual variability and concentrations of DIN, which were higher in 2011 and 2018 (Figure 5g), while across the entire NAP they were higher in 2015 and lower in 2016. High interannual variability was also observed in phosphate concentrations of up to two-fold (~1-3 µmol kg^{-1}) throughout the NAP (second column in Figure 5). The highest concentrations of phosphate were measured in 2003 in the Gerlache Strait (Figure 5b), 2010 in the western basin of Bransfield Strait (Figure 5e), and 2011 in the central basin of Bransfield Strait (Figure 5h), and the lowest in 2008 in the eastern basin of Bransfield Strait (Figure 5k) and 2014 in both Gerlache Strait (Figure 5b) and the western basin of Bransfield Strait (Figure 5e).

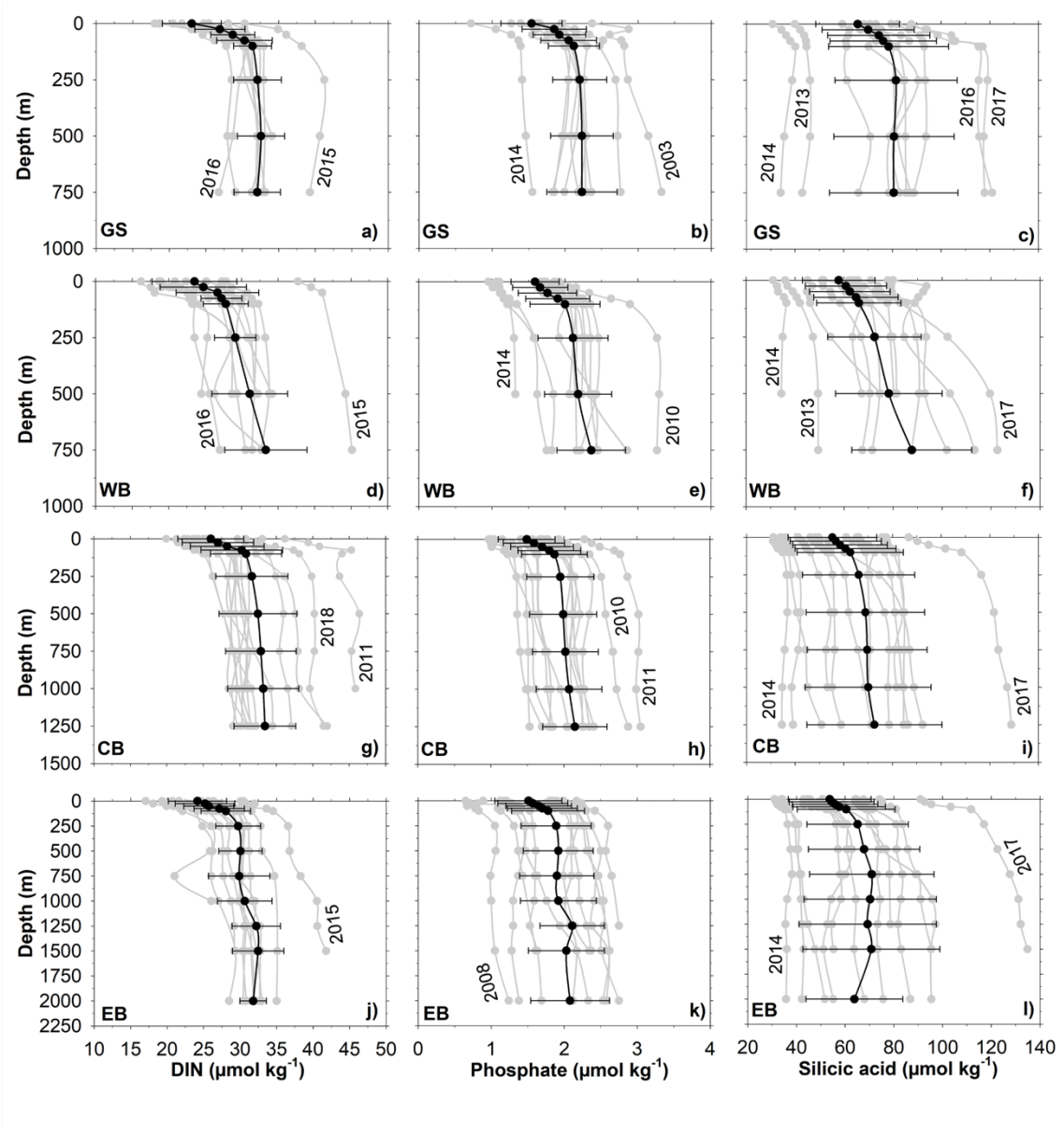

Figure 5: Summer (Jan-Mar) averaged profiles of macronutrients for each year from 1996 to 2019 along the northern Antarctic Peninsula, comprising the regions: (a-c) Gerlache Strait (GS), and the (d-f) western (WB), (g-i) central (CB) and (j-l) eastern (EB) basins of Bransfield Strait. Profiles for each year are presented in grey lines and the black lines are the averaged profiles over the period for each property and region. The horizontal black bars are the standard deviations for each depth. Years showing anomalous behaviour (i.e., outside the

standard deviation) are highlighted.

We compared the average profiles of macronutrients along the NAP during periods of positive and negative SAM or ENSO (Figure 6). In years of positive SAM there was an increase (red line profiles on positive values in Figure 6) in the concentrations of DIN (first column in Figure 6), phosphate (second column in Figure 6), and silicic acid (third column in Figure 6) through the water column along the NAP. Such an increase was more pronounced in silicic acid concentrations, mainly in the central (Figure 6i) and eastern (Figure 6l) basins of Bransfield Strait, particularly below 250 m. Although phosphate and DIN concentrations increased in all regions during positive SAM, phosphate increase was not significant in the central basin of Bransfield Strait (Figure 6h). Furthermore, there was greater uncertainty in the phosphate increase in the Gerlache Strait (Figure 6b), where the DIN increase (Figure 6a) was also not significant. Compared to SAM, there was a smaller difference in macronutrient concentrations between the years of positive and negative ENSO (blue line profiles in Figure 6). Yet, higher differences were observed in the central (Figure 6g-i) and eastern (Figure 6j-l) basins of Bransfield Strait, where macronutrient concentrations were lower during positive ENSO. Silicic acid concentrations were lower during positive ENSO in all regions, but the differences were not significant. On the other hand, there was a significant decrease in DIN in the central (Figure 6g) and eastern (Figure 6j) basins of Bransfield Strait, while DIN increased in the western basin (Figure 6d). In addition, there was a significant increase in phosphate during years of positive ENSO in the Gerlache Strait (Figure 6b) and the western basin of Bransfield Strait (Figure 6e), while in the eastern basin phosphate concentrations decreased (Figure 6k).

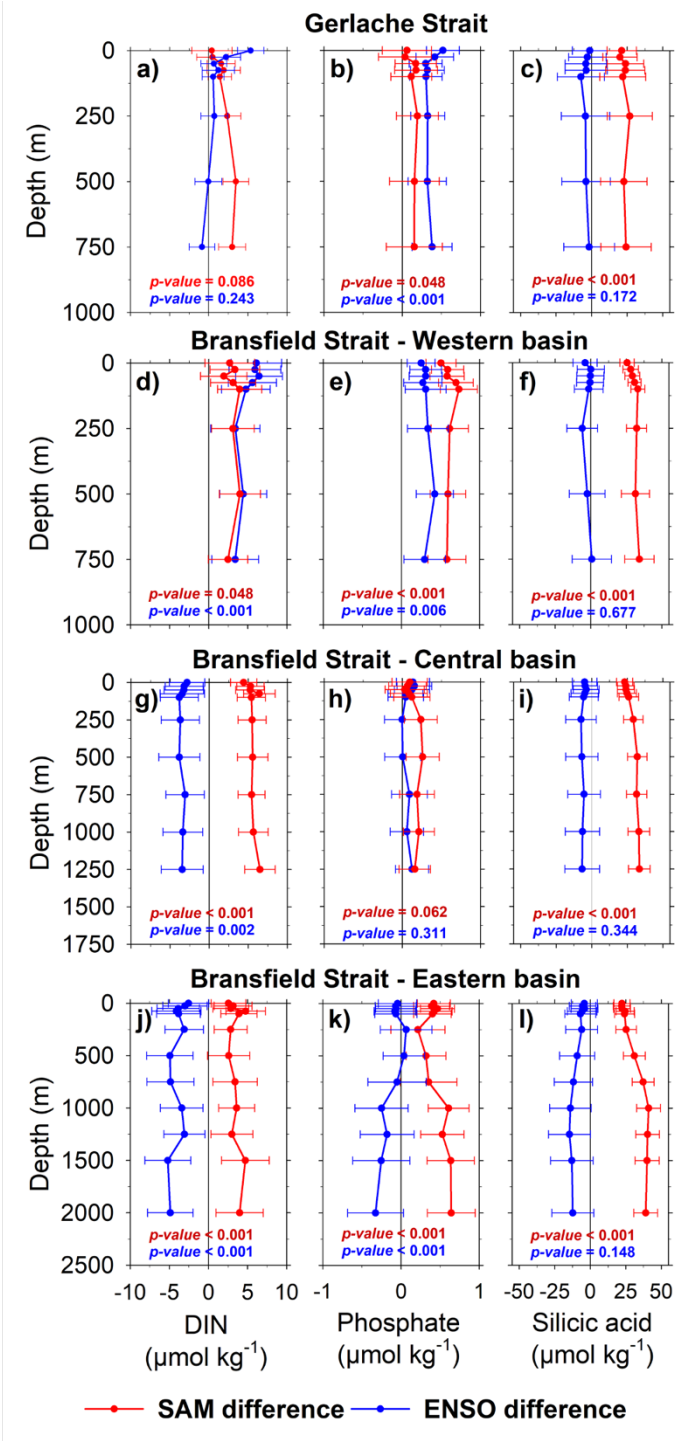
Gerlache Strait
Bransfield Strait - Western basin
Bransfield Strait - Central basin
Bransfield Strait - Eastern basin
Depth (m)
a)
b)
c)
d)
e)
f)
g)
h)
i)
j)
k)
l)
p-value = 0.086
p-value = 0.243
p-value = 0.048
p-value < 0.001
p-value < 0.001
p-value = 0.172
p-value = 0.048
p-value < 0.001
p-value < 0.001
p-value = 0.006
p-value < 0.001
p-value = 0.677
p-value < 0.001
p-value = 0.002
p-value = 0.062
p-value = 0.311
p-value < 0.001
p-value = 0.344
p-value < 0.001
p-value < 0.001
p-value < 0.001
p-value < 0.001
p-value < 0.001
p-value = 0.148
DIN (µmol kg-1)
Phosphate (µmol kg-1)
Silicic acid (µmol kg-1)
SAM difference
ENSO difference

Figure 6: Influence of Southern Annular Mode (SAM) and El Niño-Southern Oscillation (ENSO) modes of climate variability on the average profiles of macronutrients along the northern Antarctic Peninsula, comprising the regions: (a-c) Gerlache Strait, and the (d-f) western, (g-i) central and (j-l) eastern basins of Bransfield Strait. In red the difference in average profiles between positive and negative SAM is shown, while in blue the same is shown for ENSO. Positive values indicate an increase in macronutrients during positive SAM and ENSO years, while negative values indicate a decrease in macronutrients during positive SAM and ENSO years and vice versa. The horizontal bars are the propagated uncertainties in calculating the difference between the averages for each depth and the p-values refer to the statistical tests to assess the significance of the difference between the average profiles.

3.3 Uptake stoichiometry and seasonal drawdown of macronutrients

The full-depth average DIN/phosphate ratio across the NAP environments ranged from 11.8 ± 0.9 (r^2 = 0.965; $p < 0.001$) to 14.2 ± 0.7 (r^2 = 0.978; $p < 0.001$), observed in the western and eastern basins of Bransfield Strait (Figure 7a), respectively. From 2013 to 2019, when data are available for all NAP environments, the lowest DIN/phosphate ratios (< 11) were observed in 2016 along the Bransfield Strait (Table S2), while in the Gerlache Strait the lower DIN/phosphate ratio (9.40 ± 0.87; *r^2=0.95; p<0.001; n=8*) was recorded in 2019. DIN/phosphate ratios higher than 20 were observed in the western basin of Bransfield Strait in 2018 and in the eastern basin in 2017 and 2019. The average silicic acid/DIN ratio ranged from 1.7 ± 0.1 (r^2 = 0.974; $p < 0.001$) in Gerlache Strait to 3.1 ± 0.3 (r^2 = 0.956; $p < 0.001$) in the western basin of Bransfield Strait (Figure 7b). From 2013 to 2019 the lowest silicic acid/DIN ratio (< 1.2) was recorded in 2014 along the entire NAP and the highest ratios (> 3.8) were recorded in 2015 and 2017 along Bransfield Strait. A silicic acid/DIN ratio of 5.5 ± 0.5 was recorded in 2009 in the central basin of Bransfield Strait, two-fold the average for the entire period in that region (2.2 ± 0.2).

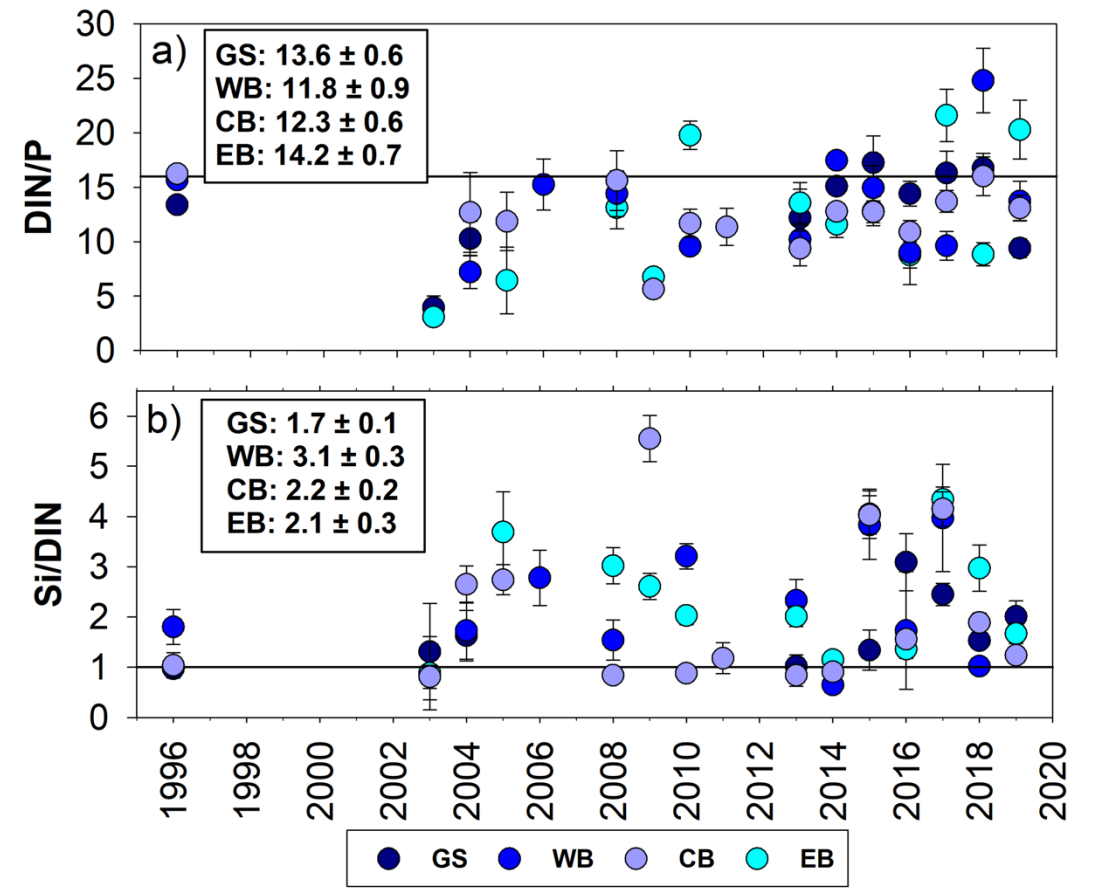

Figure 7: Time series of macronutrient uptake stoichiometry. (a) Dissolved inorganic nitrogen (DIN)/phosphate (P) and (b) silicic acid (Si)/DIN ratios during austral summer (Jan-Mar) and along the northern Antarctic Peninsula. Colours show the sub-regions studied (GS: Gerlache Strait; WB: Western Bransfield; CB: Central Bransfield; EB: Eastern Bransfield). The vertical bars are the standard error on the slope of the regression DIN versus P, and Si versus DIN. Likewise, the values shown on the inset of each plot are the (a) DIN/P and (b) Si/DIN ratios with the respective standard deviations, considering the average profiles over the period for each region (Figure 5). The solid black line marks the ratios (a) DIN/P=16 and (b) Si/DIN=1. Statistics for each year are shown in Table S2.

The seasonal drawdown in all macronutrients is characterised by a decreasing pattern from south (Gerlache Strait) to north (eastern basin of Bransfield Strait) along the NAP (Figure 8). High seasonal drawdown of phosphate was observed in 2010 in the western basin of Bransfield Strait, while higher drawdown in silicic acid was observed in 2016 and 2017 in Gerlache Strait. Seasonal drawdown of

silicic acid close to zero was observed in 2015 and 2016 in the western basin of Bransfield Strait, while for phosphate this depletion was found in 2015 in Gerlache Strait. The interannual variability in drawdown of phosphate (Figure 8b) and silicic acid (Figure 8c) concentration was high in the western basin of Bransfield Strait, while the variability in drawdown of DIN was fairly similar in all sub-regions along the NAP (Figure 8a).

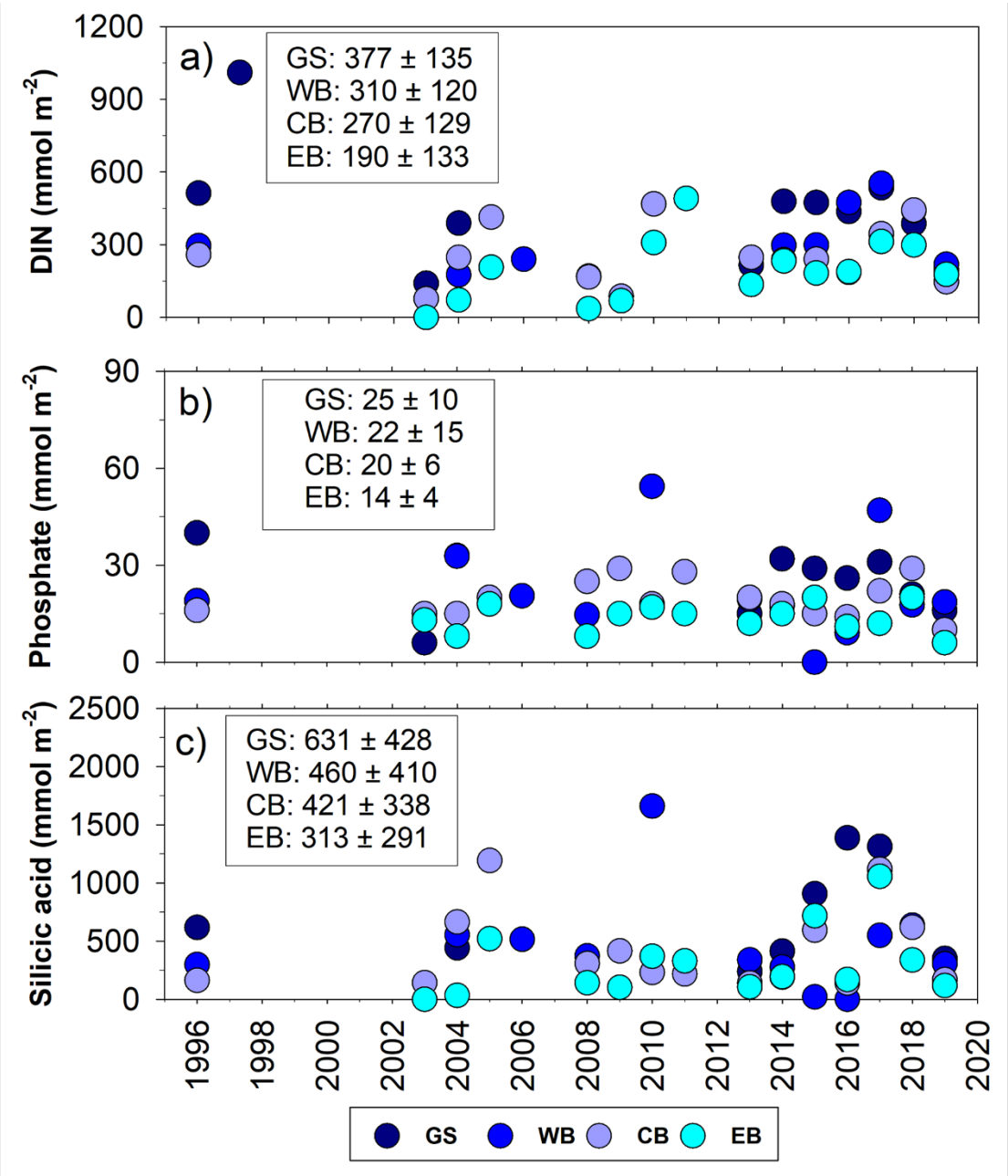

Figure 8: Time series of seasonal nutrient drawdown. (a) Dissolved inorganic nitrogen (DIN), (b) phosphate and (c) silicic acid, during austral summer (Jan-Mar) along the northern Antarctic Peninsula. Each circle represents the seasonal drawdown of each nutrient in Gerlache Strait (GS) and the western (WB), central (CB), and eastern (EB) basins of Bransfield Strait. The values shown

on the inset are the averages for the entire period with the respective standard deviations.

4. Discussion

4.1 Main sources of macronutrients for the northern Antarctic Peninsula

The main source of macronutrients for the NAP environments is the mCDW intrusions in the coastal and shelf domains (Henley et al., 2019), which carry DIN, phosphate, and silicic acid (Figures. 2 and 3) as this intermediate water intrudes onto the continental shelf (Prézelin et al, 2000; Couto et al., 2017; Venables et al., 2017). When mCDW intrudes into the shelf domains (i.e., Gerlache Strait, and western basin of Bransfield Strait), it often upwells by topographic effect (Venables et al., 2017; Parra et al., 2020), decreasing oxygen at intermediate depths and transporting macronutrients into surface waters. These waters are further advected northward by the Bransfield Current towards the eastern basin of Bransfield Strait, enriching the surface waters of the NAP with high concentrations of macronutrients. Therefore, macronutrient concentrations are mostly not exhausted in the NAP surface waters during summer, even in years with strong phytoplankton blooms (e.g., 2016, Costa et al., 2020, 2021). Although the mCDW is also an important source of macronutrients for the western Antarctic Peninsula (WAP) south of the NAP (Prézelin et al., 2000; Klinck et al., 2004; Henley et al., 2019), surface waters almost exhausted with respect to DIN and phosphate have been recorded in summer over the WAP continental shelf (Henley et al., 2017, 2018). However, along the NAP surface, concentrations of DIN and phosphate were not lower than 15 and 0.5 µmol kg^{-1}, respectively (Figures 5 and S6a,d). This is likely because both Gerlache Strait and the western basin of Bransfield Strait are regions more exposed to the ACC influence, which probably facilitate more frequent intrusions of mCDW (García et al., 2002; Parra et al., 2020), favouring higher supply of macronutrients into the surface layer through topographic upwelling and advective mixing. For example, high sea surface concentrations of nitrate (12-24 µmol kg^{-1}) and phosphate (1.0-1.6 µmol kg^{-1}) are observed offshore the WAP (Hauri et al., 2015), under strong influence of the ACC that carries CDW. Indeed, at Palmer Station region, in the southernmost part of the NAP, mCDW is expected to exert a strong and constant influence on macronutrient supply (Figure 9; Prézelin et al., 2000; Kim et al., 2016). In both the NAP (Figure 5 c,f,i,l) and near Palmer Station region (Figure S6g), the surface concentrations of silicic acid are higher than 50 µmol kg^{-1}. This is likely due to the local terrestrial sources of silicic acid in both regions (e.g., Hawkings et al., 2017), further supplementing the high silicic acid input from mCDW (see section 4.2 below). Indeed, the surface silicic acid concentration at Palmer Station region (69.0 ± 10.4 µmol kg^{-1}, Figure S6a) is higher than that found along the NAP (third column in Figure 5). In both regions, such concentrations are even higher than those found in the northwest Weddell Sea (Hoppema et al., 2015), where the direct influence of mCDW is comparatively small.

CDW is sourced from North Atlantic Deep Water (e.g., Ferreira & Kerr, 2017),

so it has had a long period over which remineralised organic matter has accumulated and hence high concentrations of macronutrients. Along the NAP, this is even more evident in the concentrations of phosphate (Figure 2e) and silicic acid, whose concentrations are up to 50% higher under the influence of mCDW in the Gerlache Strait and western basin of Bransfield Strait than in the rest of the NAP (Figure 2f). The central basin of Bransfield Strait is strongly influenced by DSW from the Weddell Sea in the deep layers (> 800 m; Dotto et al., 2016; Damini et al., 2022; Wang et al., 2022), where there are higher concentrations of DIN (Figure 2d), phosphate (Figure 2e) and dissolved oxygen (Figure 2c) associated with lower concentrations of silicic acid (Figures 2f and 9). This is a result of the slower rate of opal dissolution, as diatom frustules sink out of the surface layer, compared to the remineralisation of sinking organic matter (Brown et al., 2006) that releases DIN and phosphate (Hoppema et al., 2015). Indeed, phytoplankton blooms recorded in the northwestern Weddell Sea are often composed mostly (> 80%) of diatoms (Mendes et al., 2012), associated with low DIN/phosphate uptake ratios (< 14) and high silicic acid/DIN ratios (> 1) (Flynn et al., 2021). Due to the marked depletion of silicic acid during diatom growth, the DSW from the Weddell Sea is relatively low in silicic acid while the concentrations of DIN and phosphate are increased by remineralisation of sinking organic matter as it is advected towards the NAP. This is reinforced by the low DIN/phosphate uptake ratios (< 16, Fig 7a) and high silicic acid/DIN uptake ratios (> 2, Fig 7b) along the NAP, although there is great interannual variability in these ratios. The advection time of shelf waters from the Weddell Sea towards the Bransfield Strait is estimated to be between 1 and 5 months to reach the central basin (van Caspel et al., 2018; Damini et al., 2022). This time should not be enough to release high silicic acid concentrations from late spring diatom blooms. Thus, the interannual variability in nutrient concentrations driven by DSW advection is likely due to variability in the advection time of these waters and in the timing and duration of diatom blooms, from early spring to summer. The influence of mCDW and DSW from the Weddell Sea on silicic acid concentrations is most evident when we estimate the contribution of these waters along the NAP from the silicic acid versus dissolved oxygen mixing diagram (Figure 9). Below 50 m, the southern end of the NAP (near Palmer Station) is strongly influenced by the silicic acid-rich and dissolved oxygen-poor mCDW. Conversely, the central basin of Bransfield Strait is strongly influenced by the high dissolved oxygen and low silicic acid DSW. This west-east pattern in the fractional contributions of mCDW and DSW to the total mixture is very close to the estimates determined by Damini et al. (2022) in the region. For the deep layers (i.e., > 800 m) of central basin of Bransfield Strait, those authors estimated an averaged contribution of 31 ± 9 % of mCDW and 69 ± 9 % of DSW, while for the eastern basin of Bransfield Strait the averaged contribution to the mixture was 44 ± 8 % for mCDW and 56 ± 8 for DSW. Although the Palmer Station region is made up of almost 100 % mCDW below 50 m (Figure 9), silicic acid concentrations are higher than those expected only from mCDW input, revealing that there are important local sources of silicic acid in this region.

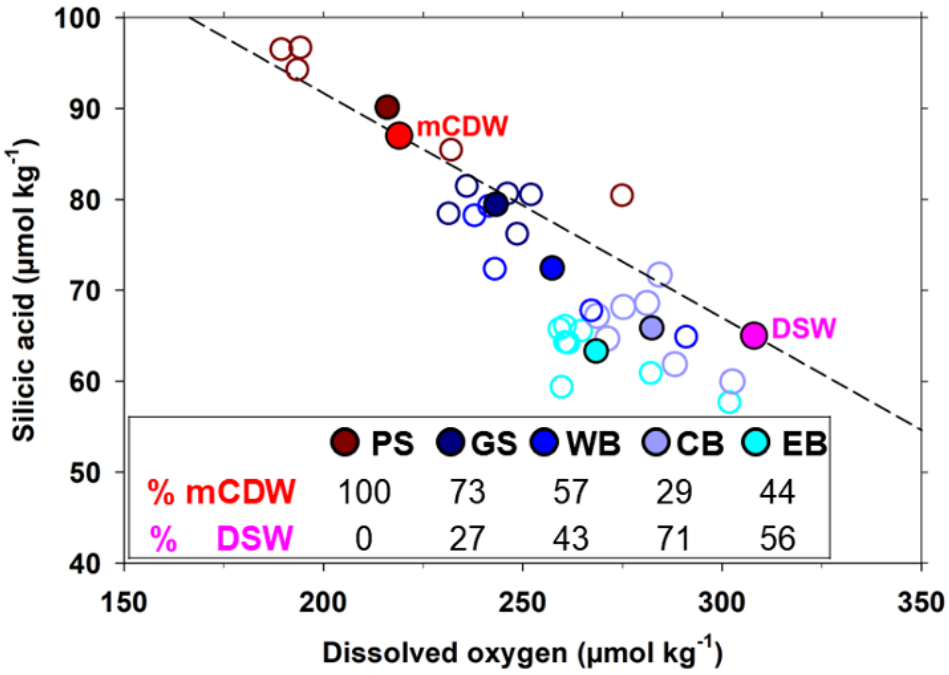

Figure 9: Influence of the mixture between modified Circumpolar Deep Water (mCDW) and Dense Shelf Water (DSW) from the Weddell Sea on dissolved oxygen and silicic acid below 50 m along the northern Antarctic Peninsula. Open circles represent the average concentrations of dissolved oxygen and silicic acid for each depth interval below 50 m and closed circles indicate the average through the water column below 50 m at Palmer Station (PS), Gerlache Strait (GS) and the western (WB), central (CB) and eastern (EB) basins of Bransfield Strait. The data used here are from the profiles shown in Figures 4 and 5. For PS we used dissolved oxygen (Waite, 2022) and silicic acid (Ducklow et al., 2019) data from the U.S. Palmer Station (Figure 1). The dissolved oxygen concentration endmembers were 219 µmol kg^{-1} for mCDW (red closed circle) and 308 µmol kg^{-1} for DSW (blue closed circle), from Damini et al. (2022). The silicic acid concentration endmembers were 87 µmol kg^{-1} (Cape et al., 2019) for mCDW and 65 µmol kg^{-1} (Hoppema et al., 2015) for DSW.

4.2 Additional sources of macronutrients for the northern Antarctic Peninsula

In fact, local sources of macronutrients are also important along the NAP. Terrestrial input of iron (De Jong et al., 2012; Hatta et al., 2013; Annett et al., 2017; Sherrell et al., 2018) and silicic acid (e.g., Hawkings et al., 2017) is well known over the Antarctic continental shelf. However, intense phytoplankton booms in fjords that flow into the NAP (e.g., Mascioni et al., 2021; Forsch et

al., 2021) can inject high concentrations of remineralised DIN and phosphate into downstream regions. Moreover, the abrupt freshwater inflow from fjords increases the upper ocean stability and fertilises the region with iron (Forsch et al., 2021), triggering intense phytoplankton blooms downstream. Likewise, such favourable conditions for intense phytoplankton growth, mainly diatoms, are also triggered by glacial (Höfer et al., 2019; Wang et al., 2020; Meredith et al., 2022) and sea ice melting (Mendes et al., 2018; Brown et al., 2019; Costa et al., 2020). Such high primary productivity sustains a high zooplankton density (e.g., Henley et al., 2019; Plum et al., 2020), which intensifies the remineralised nutrient stocks (Alcaraz et al., 1998; Whitehouse et al., 2011; Ratnarajah & Bowie, 2016; Plum et al., 2020) locally and further advected along the NAP. Furthermore, the eastern basin of Bransfield Strait is an important pathway of icebergs released from the Weddell Sea (Collares et al., 2018; Barbat & Mata, 2021), which transport iron (Hopwood et al., 2017; Laufkötter et al., 2018) and likely silicic acid (Höfer et al., 2019) from the eastern shelf of the Antarctic Peninsula into the NAP. Hence, there is an increased supply of silicic acid in the eastern basin of Bransfield Strait (Figure 2f), where there are also episodic intrusions of silicic acid-enriched mCDW at intermediate levels (Dotto et al., 2016; Damini et al., 2022). Although widely neglected in biogeochemical studies (Jones et al., 2015), mesoscale eddies may have a relevant impact on nutrient supply along the NAP. Such structures can favour nutrient supply via upwelling of waters enriched with remineralised material (Jones et al., 2015) and by intensifying remineralisation by deepening the mixed layer depth within the eddies (Dufois et al., 2014). Moreover, eddies can trap advected water masses (Thompson & Heywood, 2009) with high remineralised material content (Dufois et al., 2014), such as modified Warm Deep Water (a mixture of CDW with Winter Water in the Weddell Sea) (Hoppema et al., 2015).

The high concentration of macronutrients (Figure 2) and the supply of iron (Ardelan et al., 2010; Annett et al., 2017; Sherrell et al., 2018) coupled with the increased upper ocean stability driven by sea ice melting and/or glacial freshwater input during the summer supports high productivity along the NAP (Mendes et al., 2018; Höfer et al., 2019; Costa et al., 2020). We found an average DIN/phosphate uptake ratio (Figure 7a) within the expected range for the NAP (~13-21, Henley et al., 2019), supporting the observations that diatoms are the dominant group composing high biomass phytoplankton blooms (Mendes et al., 2008; van Leeuwe et al., 2020; Costa et al., 2020, 2021). In the Southern Ocean, lower DIN/phosphate ratios (<16) have been observed during diatom blooms, while other smaller phytoplankton groups are associated with a higher (> 16) ratio (Arrigo et al., 1999; Henley et al., 2019, 2020). This is particularly true along the NAP, where we observed low DIN/phosphate uptake ratios (< 16, Figure 7a) when the phytoplankton composition was dominated by diatoms (Figure S7). For example, a low DIN/phosphate uptake ratio was observed in 2016 along the NAP (Table S2), when an intense phytoplankton bloom was recorded (Costa et al., 2020, 2021) and over 90% of it was composed of diatoms (Figure S7). Conversely, there were high DIN/phosphate ratios (> 20; Figure

7a) when phytoplankton composition was dominated by other smaller groups, such as dinoflagellates, haptophytes (*Phaeocystis antarctica*), cryptophytes and green flagellates, in 2017 along the NAP and in 2018 in the western basin of Bransfield Strait (Figure S7). However, we found even lower DIN/phosphate uptake ratios (< 9) in some years (Figure 7a), indicating possible additional sources of phosphate in relation to DIN. This may be associated with the release of phosphate accumulated in sea ice (Fripiat et al., 2017), although its effect on the water column remains unclear (Henley et al., 2019). Moreover, the high density of krill enriched by diatom blooms (Henley et al., 2020) may favour phosphate supply, as krill release phosphate and ammonium through grazing and excretion processes (Tovar-Sanchez et al., 2007). We identified silicic acid/DIN ratios that were within the range previously observed along the WAP and at Palmer Station (1-3; Henley et al., 2019; Kim et al., 2016). Silicic acid/DIN ratios higher than 1 have been associated with diatoms growing under iron-limited conditions (Henley et al., 2019, 2020), but the NAP is not expected to experience iron limitation (De Jong et al., 2012; Hatta et al., 2013; Kim et al., 2016; Annett et al., 2017; Sherrell et al., 2018). The higher silicic acid/DIN uptake ratios are likely to be a result of high silicic acid concentrations being supplied by mCDW intrusions and local remineralisation/dissolution of diatoms walls. The intense diatom blooms in early spring can lead to a depletion in silicic acid in the upper ocean (Kim et al., 2016) and then opal dissolution increases the silicic acid concentration again towards summer. Indeed, we found the highest silicic acid/DIN ratio and the lowest DIN/phosphate ratio in the western basin of Bransfield Strait (Figure 7), where there is a great influence of mCDW intrusions (Figure 2) and intense diatom-dominated blooms (Álvarez et al., 2002; Costa et al., 2020).

4.3 Drivers of interannual variability of macronutrients along the northern Antarctic Peninsula

The huge interannual variability in nutrient concentrations along the NAP is driven mainly by the relative strength of mCDW intrusions and the advection of DSW from the Weddell Sea. During positive SAM, westerly winds are intensified southward (Marshall et al., 2006; Dinniman et al., 2012), strengthening mCDW intrusions along the NAP (Barllet et al., 2018; Damini et al., 2022; Wang et al., 2022) and increasing nutrient concentration. In addition to direct nutrient input, greater vertical mixing leads to an increased supply of organic matter (da Cunha et al, 2018; Avelina et al., 2020) and a consequent increase in remineralised nutrient concentrations throughout the water column. Overall, the influence of SAM on nutrient concentrations is more evident in the central and eastern basins of Bransfield Strait because these regions are more influenced by DSW from the Weddell Sea than both the western basin of Bransfield Strait and Gerlache Strait (Barllet et al., 2018; Damini et al., 2022; Wang et al., 2022). In these regions, greater differences between positive/negative SAM are observed in silicic acid concentrations because DSW (mCDW) is depleted (enriched) in silicic acid (Figure 9). During positive SAM, DSW advection into Bransfield Strait is weakened, while mCDW intrusion is strengthened (Wang et al., 2022),

increasing the difference between greater/lesser influence of these distinct water masses. On the other hand, the influence of DSW is smaller in the western basin of Bransfield Strait and the Gerlache Strait (Wang et al., 2022), decreasing the silicic acid depletion due to DSW advection. This is supported by the lower influence of SAM on phosphate and DIN concentrations in Gerlache Strait (Figure 6), as the time for organic matter remineralisation is likely shorter than the advection time for DSW to reach this region.

Conversely, during positive ENSO, westerly winds typically migrate northward (Stammerjohn et al., 2008) and weaken mCDW intrusions over the NAP (Barllet et al., 2018; Damini et al., 2022), decreasing nutrient supply. Such conditions strengthen the extent of the DSW advected from the Weddell Sea, reaching the southern end of the NAP (i.e., Gerlache Strait, Wang et al., 2022). Since DSW is enriched in DIN and phosphate (Figure 2d,e) and contains lower concentrations of silicic acid (Figure 2f), the interannual variability in silicic acid concentrations is intensified over the NAP. Indeed, we observed a 57% decrease in silicic acid from 2015 (a year of positive SAM) to 2016 (a year of strong positive ENSO) in the central basin of Bransfield Strait, where significant changes were also observed in organic carbon concentrations between these two years (Avelina et al., 2020). The influence of ENSO on nutrient concentrations is minor compared to SAM (Figure 6) because DSW also contains high concentrations of DIN and phosphate. Moreover, variations in ENSO are expected to exert less influence on circulation along the NAP than variations in SAM (e.g., Wang et al., 2022). This may be associated with uncertainties in the circulation response time to ENSO variations (i.e., 6 to 9 months; Meredith et al., 2008; Barlett et al, 2018; Dotto et al., 2016) and DSW advection time along the NAP, which are still a challenge to understand. The DSW is estimated to take around 1 to 5 months to reach the central basin of Bransfield Strait (van Caspel et al., 2018; Damini et al., 2022). The period of around 5 months is consistent with the estimated time for the drift of medium-sized icebergs from the northwestern Weddell Sea to reach the central basin of Bransfield Strait (Collares et al., 2018). However, its interannual variability and sensitivity to SAM and ENSO events, as well as the residence time of the waters within Bransfield Strait remain unclear. Nutrient concentrations appear to be more sensitive to ENSO in the eastern basin of Bransfield Strait (Figure 6) because this is the main pathway of DSW input into the NAP (van Caspel et al., 2018; Wang et al., 2022). Therefore, it is reasonable to conclude that the high interannual variability in nutrient concentrations along the NAP is driven mainly by changes in ocean circulation and water mass mixing caused by strong variability in the SAM. The effect of ENSO variability on silicic acid concentrations via advected DSW is more evident while its effect on DIN and phosphate concentrations is often counteracted because DIN and phosphate are also high in DSW.

In addition, the effects of SAM and ENSO on the biogeochemistry of waters along the NAP can either superimpose or counteract each other, depending on whether the region experiences concomitant periods of positive SAM and positive ENSO or vice versa (e.g., Stammerjohn et al., 2008). Regarding our results,

unfortunately, we could not accurately assess these combined effects because we only have a more robust time series in the last decade when the Southern Ocean has been experiencing successive positive SAM (e.g., Keppler et al., 2019) and negative ENSO conditions (Santoso et al., 2017). Moreover, extreme events can trigger processes that change the concentration of macronutrients over different time scales. For example, the anomalously high silicic acid concentrations in 2017 (Figure 5), mainly noted in the central and eastern basins of Bransfield Strait, may have been a result of massive diatom blooms triggered by the intense positive ENSO during 2016 (e.g., Costa et al., 2020, 2021), which were subsequently remineralised. Although they were recorded during the summer of 2016, reaching chlorophyll *a* concentrations > 45 mg m^{-3} with more than 95% composed of diatoms (e.g., Costa et al., 2020), these blooms are thought to occur over a wider temporal window, including early austral spring (Gonçalves-Araujo et al., 2015; Ferreira et al., 2020). Therefore, these anomalously high concentrations of silicic acid in 2017 may be a result of subsequent remineralisation of the intense diatom blooms during 2016. In fact, silica concentrations as high as 110 µmol kg^{-1} have been recorded above 150 m in this region, associated with high diatom biomass in the 1980s (Heywood & Priddle, 1987). Nevertheless, such an anomalous increase in silicic acid likely was the result of an additional supply besides the remineralisation of diatom blooms, as DIN and phosphate concentrations were not anomalously high. Although it is unclear what the additional sources of silicic acid there were in this year, these could be linked to other extreme events during 2016. Since March 2016, an iceberg with an area of approximately 10% of the Larsen-C Ice Shelf began its calving process until it was calved off the ice shelf in July 2017 (Hogg & Gudmundsson, 2017). Since continental ice can be an important source of silicic acid to the polar oceans (Hawkings et al., 2017), the calving process of this iceberg may have been one of the additional sources of silicic acid for the NAP. Furthermore, a dramatic switch from the strong positive SAM index in September to the strong negative SAM index in November 2016 favoured a 3°C anomalous increase in air temperature over the Weddell Sea (Turner et al., 2020). This rapid change has led to a record reduction in sea ice extent in the Weddell Sea since the satellite era began (Turner et al., 2020). Both the strong positive SAM index and the reduction in sea ice extent may have intensified the influence of modified Warm Deep Water with high silicic acid concentrations (> 125 µmol kg^{-1}; Hoppema et al., 2015) in the northwestern Weddell Sea. Hence, part of the anomalous increase in silicic acid in 2017 may be associated with this chain of extreme events, as modified Warm Deep Water influences the waters that are advected to the Bransfield Strait (e.g., van Caspel et al., 2018; Barlett et al., 2018). We cannot account for the impact of each event on the additional increase in silicic acid. However, this increase is more likely to be associated with events in the Weddell Sea, as the highest concentrations were recorded in the central and eastern basins of Bransfield Strait (Figure 5). This suggests that the calving process of the giant iceberg from the Larsen-C Ice Shelf probably had a greater impact on silicic acid concentrations due to input from sediments on the shallow continental shelf.

4.4. Seasonal macronutrients drawdown

Despite the high concentration of macronutrients that we observed throughout the NAP environments, supporting high primary productivity, Gerlache Strait and the western basin of Bransfield Strait appear to be the most favourable regions for strong phytoplankton growth. Seasonal nutrient drawdown in these regions is nearly double that observed in the rest of the NAP (Figure 8). There is a clear south-north decreasing gradient in seasonal nutrient drawdown along the NAP. Even in the Gerlache Strait, where the seasonal drawdown is higher (Figure 8), it is lower than that found at the Palmer Station region (Kim et al., 2016) and further south along the WAP (Henley et al., 2017, 2018). The relatively lower seasonal drawdown of macronutrients, reaching values close to zero (Figure 8) along the NAP, occurs because the surrounding environments are more exposed regions, prone to be influenced by mCDW intrusions (García et al., 2002; Parra et al., 2020) and normally show a high degree of mixing in the water column structure. However, as Gerlache Strait and the western basin of Bransfield Strait are shallower, more enclosed areas, and closer to the coast, they are more likely to experience increased upper ocean stability as a result of sea ice melting and glacial freshwater input. Such conditions are favourable to phytoplankton blooms (Costa et al., 2020; Ferreira et al., 2022) and, therefore, to greater seasonal drawdown of macronutrients. As the summer phytoplankton blooms in these regions are dominated by diatoms (Costa et al., 2020, 2021; Ferreira et al., 2022), which are known to enhance CO_2 uptake (Brown et al., 2019; Costa et al., 2020), these regions also act as a strong summer atmospheric CO_2 sink (Monteiro et al., 2020a,b). The dominance of phytoplankton growth either by diatoms or smaller cells was thought to act as an additional control factor over the magnitude of CO_2 uptake in Gerlache Strait (Kerr et al., 2018c). In fact, the highest seasonal drawdown of silicic acid was recorded in Gerlache Strait in 2016 (Figure 8c), when there was an intense diatom bloom (Costa et al., 2020) and the strongest summer CO_2 uptake since 1999 (Monteiro et al., 2020a,b). The great interannual variability in seasonal nutrient drawdown must also be driven to some extent by winter sea ice cover (Kim et al., 2016; Henley et al., 2017). During the negative SAM condition, increased winter sea ice cover enhances the upper ocean stability driving phytoplankton blooms in the following summer (Saba et al., 2014), increasing the seasonal nutrient drawdown (Kim et al., 2016). Moreover, diatom blooms can be strengthened by the release of diatom cells residing within the sea ice when there is intense sea ice melting during the summer (Kim et al., 2016). Hence, part of the high interannual variability in nutrient concentration associated with the SAM and ENSO climate modes along the NAP must be driven by the oscillation in sea ice extent, which is also driven by SAM and ENSO.

5. Conclusions

High concentrations of macronutrients (DIN, phosphate, and silicic acid) were recorded during austral summer in environments along the NAP. The macronutrient concentrations exhibited huge interannual variability, reaching up to

three-fold changes in silicic acid and two-fold changes in phosphate concentrations among the annually-averaged profiles for each region. The coupling of mCDW intrusions together with local sources, such as remineralisation of organic matter, terrigenous inputs of silicic acid, mesoscale structures and circulation, and sea ice dynamics, explains the high nutrient concentrations found along the NAP. The great interannual variability is also driven largely by the extent of mCDW intrusions and its mixing with the DSW advected from the Weddell Sea, which can be intensified by local mesoscale processes. The strength of mCDW intrusions, and hence nutrient supply, is often modulated by the SAM, and to a lesser extent by ENSO. However, further studies are still needed to better decouple their influences on changes in the mixture between mCDW and DSW. In addition, we found stoichiometric uptake ratios of DIN/phosphate less than 16 and silicic acid/DIN greater than 1, associated with high phytoplankton biomass, mainly composed of diatoms, which have been associated to strong CO_2 uptake in the coastal and relatively shallow zone of the NAP. Despite the enhanced summer phytoplankton growth, relatively low seasonal nutrient drawdown was found in most sub-regions of the NAP, reaching down to near-zero drawdown for phosphate and silicic acid. This is likely due to the high supply of macronutrients from different sources, which makes NAP environments highly favourable for growth and development of phytoplankton blooms. This is particularly important as the NAP is one of the most productive regions in the Southern Ocean and where major climate-driven change is being observed. Hence, these findings are critical to improving our understanding of the natural variability of Southern Ocean ecosystems and informing our predictions of how these nutrient inputs may respond to ongoing and expected climate and environmental change.

Acknowledgements

This study contributes to the activities of the CARBON Team (www.carbonteam.furg.br), the Brazilian Ocean Acidification Network (BrOA; www.broa.furg.br) and the Brazilian High Latitude Oceanography Group (GOAL; www.goal.furg.br), which is part of the Brazilian Antarctic Program (PROANTAR). GOAL has been funded by and/or has received logistical support from the Brazilian Ministry of the Environment (MMA), the Brazilian Ministry of Science, Technology, and Innovation (MCTI), the Brazilian Navy, the Secretariat of the Interministerial Commission for the Resources of the Sea (SECIRM), and the Council for Research and Scientific Development of Brazil (CNPq) through grants from the Brazilian National Institute of Science and Technology of Cryosphere (INCT-CRIOSFERA; CNPq Grants Nos. 573720/2008-8 and 465680/2014-3; FAPERGS Grant no. 17/2551-0000518-0), NAUTILUS, INTERBIOTA, PROVOCCAR and ECOPELAGOS projects (CNPq Grants Nos. 405869/2013-4, 407889/2013-2, 442628/2018-8 and 442637/2018-7, respectively), and Higher Education Personnel Improvement Coordination (CAPES Grant No. 23038.001421/2014-30). T.M. received financial support from the Brazilian Improving Coordination of Higher Education Personnel (CAPES, PhD Grant No. 88887.360799/2019-00), and from CNPq Grant No. 200649/2020-5

for an abroad PhD period supervised by S.H. R.K. received financial support from CNPq researcher Grant Nos. 304937/2018-5 and 309978/2021-1. We are thankful for the support provided by CAPES to the Graduate Program in Oceanology and the FURG project CAPES-PrInt. We appreciate the availability of high-quality data from GLODAP (https://www.glodap.info/).

Data Availability Statement

The data that support the findings of this study are published openly at https://doi.org/10.5281/zenodo.7384423.

References

Ardelan, M. V. 2010. Natural iron enrichment around the Antarctic Peninsula in the Southern Ocean, Biogeosciences, 7, 11–25. https://doi.org/10.5194/bg-7-11-2010.

Alcaraz, M. et al. Antarctic zooplankton metabolism: carbon requirements and ammonium excretion of salps and crustacean zooplankton in the vicinity of the Bransfield Strait during January 1994. J. Mar. Syst. 17, 347–359 (1998).

Álvarez, M., Ríos, A. F. & Rosón, G. Spatio-temporal variability of air–sea fluxes of carbon dioxide and oxygen in the Bransfield and Gerlache Straits during. Dee. Res. 49, 643–662 (2002).

Aminot, A. & Chaussepied, M. Manuel des analyses chimiques en milieu marin. Centre National pour L'Exploitation des Oceans (CNEXO, Brest, 1983).

Annett, A.L., Fitzsimmons, J.N., Séguret, M.J.M., Lagerström, M., Meredith, M.P., Schofield, O., Sherrell, R.M., 2017. Controls on dissolved and particulate iron dis- tributions in surface waters of the Western Antarctic Peninsula shelf. Mar. Chem. 196, 81–97.

Arrigo, Kevin R., et al. "Phytoplankton community structure and the drawdown of nutrients and CO2 in the Southern Ocean." Science 283.5400 (1999): 365-367.

Avelina, R. et al. Contrasting dissolved organic carbon concentrations in the Bransfield Strait, northern Antarctic Peninsula: insights into Enso and Sam effects. J. Marine Syst. In press (2020).

Barbat, M. M. & Mata, M. M. 2021. Iceberg drift and melting rates in the northwestern Weddell Sea, Antarctica: Novel automated regional estimates through machine learning. An. Acad. Bras. Ciênc. 94. https://doi.org/10.1590/0001-3765202220211586.

Barlett, E. M. R., Tosonotto, G. V., Piola, A. R., Sierra, M. E., and Mata, M. M. (2018). On the temporal variability of intermediate and deep waters in the Western Basin of the Bransfield Strait. Deep Sea Res. Part II Top. Stud. Oceanogr. 149, 31–46. doi: 10.1016/j.dsr2.2017.12.010.

Brown, L., Sanders, R., Savidge, G., 2006. Relative mineralisation of C and Si

from biogenic particulate matter in the upper water column during the Northeast Atlantic diatom bloom in spring 2001. J. Mar. Syst. 63, 79–90.

Brown, M. S., Munro, D. R., Feehan, C. J., Sweeney, C., Ducklow, H. W., and Schofield, O. M. (2019). Enhanced oceanic CO2 uptake along the rapidly changing West Antarctic Peninsula. Nat. Clim. Change 9, 678–683. doi: 10.1038/s41558-019-0552-3.

Cape, M. R. et al. Circumpolar deep water impacts glacial meltwater export and coastal biogeochemical cycling along the West Antarctic Peninsula. Front. Mar. Sci. 6, 144 (2019).

Collares, L. L., Mata, M. M., Kerr, R., Arigony-Neto, J., Barbat, M. M. 2018. Iceberg drift and ocean circulation in the northwestern Weddell Sea, Antarctica. Deep Res Part II Top Stud Oceanogr 149: 10-24.

Costa RR, Mendes CRB, Ferreira, A, Tavano VM, Dotto TS & Secchi ER. 2021. Large diatom bloom off the Antarctic Peninsula during cool conditions associated with 2015/2016 El Niño. Commun Earth Environ 2: 252.

Costa, R. R. et al. Dynamics of an intense diatom bloom in the Northern Antarctic Peninsula, February 2016. Limnol. Oceanogr. 66, 1–20 (2020).

Couto, N., Martinson, D. G., Kohut, J. & Schofield, O. Distribution of upper circumpolar deep water on the warming continental shelf of the West Antarctic Peninsula. J. Geophys. Res. Oceans 122, 5306–5315 (2017).

Cook, A. J. et al. 2016. Ocean forcing of glacier retreat in the western Antarctic Peninsula. Science 353, 283–286. 10.1126/science.aae0017.

Dalla Rosa, L. et al. Movements of satellite-monitored humpback whales on their feeding ground along the Antarctic Peninsula. Polar Biol. 31, 771–781 (2008). https://doi.org/10.1007/s00300-008-0415-2.

Damini, B. Y., Kerr, R., Dotto, T. S., Mata, M. M. 2022. Long-term changes on the Bransfield Strait deep water masses: Variability, drivers and connections with the northwestern Weddell Sea. Deep Sea Res Part I Oceanogr Res Pap 179: 103667.

de Baar, H. J. W., De Jong, J. T. M., Bakker, D. C. E., Löscher, B. M., Veth, C., Bathmann, U., et al. (1995). Importance of iron for plankton blooms and carbon dioxide drawdown in the Southern Ocean. Nature 373, 412–415. https://doi.org/10.1038/373412a0.

De Jong, J., Schoemann, V., Lannuzel, D., Croot, P., De Baar, H., and Tison, J.-L. (2012). Natural iron fertilization of the Atlantic sector of the Southern Ocean by continental shelf sources of the Antarctic Peninsula. J. Geophys. Res. Biogeosci. 117:G01029.

Dinniman, M. S., Klinck, J. M., & Hofmann, E. E. (2012). Sensitivity of Circumpolar Deep Water transport and ice shelf basal melt along the west Antarc-

tic Peninsula to changes in the winds. Journal of Climate, 25(14), 4799–4816. https://doi.org/10.1175/JCLI-D-11-00307.1.

Dotto, T. S., Kerr, R., Mata, M. M., & Garcia, C. A. (2016). Multi-decadal freshening and lightening in the deep waters of the Bransfield Strait, Antarctica. Journal of Geophysical Research: Oceans, 121(6), 3741–3756. https://doi.org/10.1002/2015JC011228.

Dotto, T. S., Mata, M. M., Kerr, R., & Garcia, C. A. (2021). A novel hydrographic gridded data set for the Northern Antarctic Peninsula. Earth System Science Data, 13(2), 671–696. https://doi.org/10.5194/essd-13-671-2021.

Dufois, F., N. J. Hardman-Mountford, J. Greenwood, A. J. Richardson, M. Feng, S. Herbette, and R. Matear (2014), Impact of eddies on surface chlorophyll in the South Indian Ocean, J. Geophys. Res. Oceans, 119, 8061–8077, doi:10.1002/2014JC010164.

E. Seyboth, et al. Southern Right Whale (Eubalaena australis) Reproductive Success is Influenced by Krill (Euphausia superba) Density and Climate. Sci. Rep., 6 (2016), pp. 1-8. https://doi.org/10.1038/srep28205.

Ferreira A, Costa RR, Dotto TS, Kerr R, Tavano VM, Brito AC, Brotas V, Secchi ER and Mendes CRB (2020) Changes in Phytoplankton Communities Along the Northern Antarctic Peninsula: Causes, Impacts and Research Priorities. Front. Mar. Sci. 7:576254. doi: 10.3389/fmars.2020.576254.

Ferreira, M. L. C., and Kerr, R. (2017). Source water distribution and quantification of North Atlantic deep water and Antarctic bottom water in the Atlantic Ocean. Prog. Oceanogr. 153, 66–83. doi: 10.1016/j.pocean.2017.04.003.

Flynn, R. F., Bornman, T. G., Burger, J. M., Smith, S., Spence, K. A. M., and Fawcett, S. E.: Summertime productivity and carbon export potential in the Weddell Sea, with a focus on the waters adjacent to Larsen C Ice Shelf, Biogeosciences, 18, 6031–6059, https://doi.org/10.5194/bg-18-6031-2021, 2021.

Fripiat, F. et al. (2017). Macro-nutrient concentrations in Antarctic pack ice: Overall patterns and overlooked processes. Elementa-Sci. Anthropocene 5. ht tps://doi.org/10.1525/elementa.217.

Forsch, K. O., Hahn-Woernle, L., Sherrell, R. M., Roccanova, V. J., Bu, K., Burdige, D., Vernet, M., and Barbeau, K. A.: Seasonal dispersal of fjord meltwaters as an important source of iron and manganese to coastal Antarctic phytoplankton, Biogeosciences, 18, 6349–6375, https://doi.org/10.5194/bg-18-6349-2021, 2021.

García, M. A. et al. Water masses and distribution of physico-chemical properties in the Western Bransfield Strait and Gerlache Strait during Austral summer 1995/96. Deep Sea Res. Part II Top. Stud. Oceanogr. 49, 585–602 (2002).

Gonçalves-Araujo, R. et al. Garcia Influence of oceanographic features on spatial and interannual variability of phytoplankton in the Bransfield Strait, Antarc-

tica J. Mar. Syst., 142 (2015), pp. 1-15, 10.1016/j.jmarsys.2014.09.007.

Hatta, M., Measures, C. I., Selph, K. E., Zhou, M., and Hiscock, W. T. (2013). Iron fluxes from the shelf regions near the South Shetland islands in the drake passage during the austral-winter 2006. Deep Sea Res. Part II Top. Stud. Oceanogr. 90, 89–101. doi: 10.1016/j.dsr2.2012.11.003.

Hauri, C. et al. Two decades of inorganic carbon dynamics along the West Antarctic Peninsula. Biogeosciences 12, 6761–6779 (2015).

Hawkings, J., Wadham, J., Benning, L. et al. Ice sheets as a missing source of silica to the polar oceans. Nat Commun 8, 14198 (2017). https://doi.org/10.1038/ncomms14198.

Henley SF, Cavan EL, Fawcett SE, Kerr R, Monteiro T, Sherrell RM, Bowie AR, Boyd PW, Barnes DKA, Schloss IR, Marshall T, Flynn R and Smith S (2020) Changing Biogeochemistry of the Southern Ocean and Its Ecosystem Implications. Front. Mar. Sci. 7:581. https://doi.org/10.3389/fmars.2020.00581.

Henley, S. F., Schofield, O. M., Hendry, K. R., Schloss, I. R., Steinberg, D. K., Moffat, C., et al. (2019). Variability and change in the west Antarctic Peninsula marine system: research priorities and opportunities. Prog. Oceanogr. 173, 208–237.

Henley, S.F., Jones, E.J., Venables, H.J., Meredith, M.P., Firing, Y.L., Dittrich, R., Heiser, S., Stefels, J., Dougans, J., 2018. Macronutrient and carbon supply, uptake and cy- cling across the Antarctic Peninsula shelf during summer. Philos. Trans. R. Soc. A- Math. Phys. Eng. Sci. 376. https://doi.org/10.1098/rsta.2017.0168.

Henley, S.F., Tuerena, R.E., Annett, A.L., Fallick, A.E., Meredith, M.P., Venables, H.J., Clarke, A., Ganeshram, R.S., 2017. Macronutrient supply, uptake and recycling in the coastal ocean of the west Antarctic Peninsula. Deep-Sea Res. Part II-Topical Stud. Oceanography 139, 58–76. https://doi.org/10.1016/j.dsr2.2016.10.003.

Höfer J., Giesecke R., Hopwood M. J., Carrera V., Alarcón E., González H. E. (2019). The Role of Water Column Stability and Wind Mixing in the Production/Export Dynamics of Two Bays in the Western Antarctic Peninsula. Prog. Oceanogr. 174, 105–116. doi: 10.1016/j.pocean.2019.01.005.

Hogg, A., Gudmundsson, G. Impacts of the Larsen-C Ice Shelf calving event. Nature Clim Change 7, 540–542 (2017). https://doi.org/10.1038/nclimate3359.

Hoppema, M., Bakker, K., MAC van Heuven, S., van Ooijen, J. C., and de Baar, H. J.: Distributions, trends and inter-annual variability of nutrients along a repeat section through the Weddell Sea (1996–2011), Mar. Chem., 177, 545–553, https://doi.org/10.1016/j.marchem.2015.08.007, 2015.

Hopwood, M. J., Cantoni, C., Clarke, J. S., Cozzi, S., and Achterberg, E. P. (2017). The heterogeneous nature of Fe delivery from melting icebergs.

Geochem. Perspect. Lett. 200–209. doi: 10.7185/geochemlet.1723.

Jones, E. M., Hoppema, M., Strass, V., Hauck, J., Salt, L., Ossebaar, S., et al. (2015). Mesoscale features create hotspots of carbon uptake in the Antarctic Circumpolar Current. Deep Sea Research Part II: Topical Studies in Oceanography, 138, 39– 51. https://doi.org/10.1016/j.dsr2.2015.10.006.

Keppler, L. & Landschützer, P. Regional wind variability modulates the Southern Ocean carbon sink. Sci. Rep. 9, 7384 (2019). https://doi.org/10.1038/s41598-019-43826-y.

Kerr, R. et al. Carbonate system properties in the Gerlache Strait, Northern Antarctic Peninsula (February 2015): II. Anthropogenic CO2 and seawater acidification. Deep. Res. Part II., 149 (2018b), pp. 182-192. https://doi.org/10.1016/j.dsr2.2017.07.007.

Kerr, R. et al. Carbonate system properties in the Gerlache Strait, Northern Antarctic Peninsula (February 2015): I. Sea-Air CO2 fluxes. Deep Sea Res. Part II Top. Stud. Oceanogr., 149 (2018), pp. 171-181. https://doi.org/10.1016/j.dsr2.2017.02.008.

Kerr, R. M.M. Mata, C.R.B. Mendes, E.R. Secchi. Northern Antarctic Peninsula: a marine climate hotspot of rapid changes on ecosystems and ocean dynamics. Deep Res. Part II Top. Stud. Oceanogr., 149 (2018a), pp. 4-9. https://doi.org/10.1016/j.dsr2.2018.05.006.

Khatiwala, F. Primeau, T. Hall. Reconstruction of the history of anthropogenic CO2 concentrations in the ocean. Nature, 462 (2009), pp. 346-349. https://doi.org/10.1038/nature08526.

Kim, H., Doney, S.C., Iannuzzi, R.A., Meredith, M.P., Martinson, D.G., Ducklow, H.W., 2016. Climate forcing for dynamics of dissolved inorganic nutrients at Palmer Station, Antarctica: An interdecadal (1993–2013) analysis. J. Geophys. Res.- Biogeosci. 121, 2369–2389. https://doi.org/10.1002/2015JG003311.

Klinck, J.M., Hofmann, E.E., Beardsley, R.C., Salihoglu, B., Howard, S., 2004. Water-mass properties and circulation on the west Antarctic Peninsula Continental Shelf in Austral Fall and Winter 2001. Deep-Sea Res. Part II-Topical Stud. Oceanography 51, 1925–1946. https://doi.org/10.1016/j.dsr2.2004.08.001.

Landschützer, P., et al. 2015. The reinvigoration of the Southern Ocean carbon sink. Science (80-.). 349, 1221–1224. DOI: 10.1126/science.aab262.

Laufkötter, C., Stern, A. A., John, J. G., Stock, C. A., and Dunne, J. P. (2018). Glacial iron sources stimulate the Southern Ocean carbon cycle. Geophys. Res. Lett. 13:385. https://doi.org/10.1029/2018GL079797.

Marshall, G. J. Trends in the Southern annular mode from observations and reanalyses. J. Clim., 16 (2003), pp. 4134-4143.

Marshall, G. J., Orr, A., van Lipzig, N. P. M., & King, J. C. (2006). The impact of a changing Southern Hemisphere annular mode on Antarctic

Peninsula summer temperatures. Journal of Climate, 19(20), 5388– 5404. https://doi.org/10.1175/JCLI3844.1.

Mascioni, M. et al. Microplanktonic diatom assemblages dominated the primary production but not the biomass in an Antarctic fjord. J. Marine Syst. 224, 103624 (2021). https://doi.org/10.1016/j.jmarsys.2021.103624.

Mata, M. M., Tavano, V. M. & García, C. A. E. 15 years sailing with the Brazilian High Latitude Oceanography Group (GOAL). Deep Res. Part II Top. Stud. Oceanogr. 149, 1–3 (2018). https://doi.org/10.1016/j.dsr2.2018.05.007.

Mendes, C. R. B., M. S. de Souza, V. M. T. Garcia, M. C. Leal, V. Brotas, and C. A. E. Garcia. 2012. Dynamics of phytoplankton communities during late summer around the tip of the Antarctic Peninsula. Deep-Sea Res. Part I Oceanogr. Res. Pap. 65: 1– 14. https://doi.org/10.1016/j.dsr.2012.03.002.

Mendes, C. R. B., V. M. Tavano, M. C. Leal, M. S. de Souza, V. Brota, and C. A. E. Garcia. 2013. Shifts in the dominance between diatoms and cryptophytes during three late summers in the Bransfield Strait (Antarctic Peninsula). Polar Biol. 36: 537– 547. doi: https://doi.org/10.1007/s00300-012-1282-4.

Mendes, C. R. B., V. M. Tavano, R. Kerr, T. S. Dotto, T. Maximiano, and E. R. Secchi. 2018. Impact of sea ice on the structure of phytoplankton communities in the northern Antarctic Peninsula. Deep-Sea Res. Part II Top. Stud. Oceanogr. 149: 111– 123. https://doi.org/10.1016/j.dsr2.2017.12.003.

Meredith, M. P. et al. On the interannual variability of ocean temperatures around South Georgia, Southern Ocean: forcing by El Niño/southern oscillation and the southern annular mode. Deep-Sea Res. II Top. Stud. Oceanogr., 55 (18–19) (2008), pp. 2007-2022. https://doi.org/10.1016/j.dsr2.2008.05.020.

Meredith, M. P., Stefels, J., & van Leeuwe, M. Marine studies at the western Antarctic Peninsula: priorities, progress and prognosis. Deep–Sea Res. Pt II, 139 (2017), pp. 1-8. https://doi.org/10.1016/j.dsr2.2017.02.002.

Meredith et al. 2022. Internal tsunamigenesis and ocean mixing driven by glacier calving in Antarctica. Science Adcances. 8, eadd0720. https://doi.org/10.1126/sciadv.add0720.

Moffat, C., & Meredith, M. (2018). Shelf–ocean exchange and hydrography west of the Antarctic peninsula: A review. Philosophical Transac- tions of the Royal Society A: Mathematical, Physical & Engineering Sciences, 376(2122), 20170164. https://doi.org/10.1098/rsta.2017.0164.

Monteiro, T., Kerr, R. & Machado, E.d. Seasonal variability of net sea-air CO2 fluxes in a coastal region of the northern Antarctic Peninsula. Sci Rep 10, 14875 (2020b). https://doi.org/10.1038/s41598-020-71814-0.

Monteiro, T., Kerr, R., Orselli, I. B. M. & Lencina-Avila, J. M. Towards an intensified summer CO2 sink behaviour in the Southern Ocean coastal regions.

Prog. Oceanogr. 183, 102267 (2020a). https://doi.org/10.1016/j.pocean.2020.102267.

Monteiro, Thiago, Kerr, Rodrigo, Pollery, Ricardo César Gonçalves, Mendes, Carlos Rafael Borges, Henley, Sian, Tavano, Virginia Maria, Garcia, Carlos Alberto Eiras, & Mata, Mauricio. (2022). BGQNAPv1.0: A summer macronutrients binned data set for the Northern Antarctic Peninsula, Southern Ocean (1.0) [Data set]. Zenodo. https://doi.org/10.5281/zenodo.7384423.

Niiler, P. P., Amos, A., & Hu, J.-H. (1991). Water masses and 200 m relative geostrophic circulation in the western Bransfield Strait region. Deep Sea Research Part A. Oceanographic Research Papers, 38(8–9), 943–959. https://doi.org/10.1016/0198-0149(91)90091-S.

Nowacek, D. P. et al. Super-aggregations of Krill and Humpback Whales in Wilhelmina Bay, Antarctic Peninsula. PLoS ONE 6, e19173 (2011). https://doi.org/10.1371/journal.pone.0019173.

Olsen, A., Lange, N., Key, R. M., Tanhua, T., Bittig, H. C., Kozyr, A., et al. (2020). An updated version of the global interior ocean biogeochem- ical data product, GLODAPv2.2020. Earth System Science Data, 12(4), 3653–3678. https://doi.org/10.5194/essd-12-3653-2020.

Orselli, I. B. M.et al. 2022. The marine carbonate system along the northern Antarctic Peninsula: current knowledge and future perspectives. An Acad Bras Cienc 94: e20210825. https://doi.org/10.1590/0001-3765202220210825.

Palmer Station Antarctica LTER and N. Waite. 2022. Merged discrete water-column data from PAL LTER research cruises along the Western Antarctic Peninsula, from 1991 to 2020. ver 1. Environmental Data Initiative. https://doi.org/10.6073/pasta/65c43a4688eccf8ca7cc3a2d07a0cc78.

Palmer Station Antarctica LTER, H. Ducklow, M. Vernet, and B. Prezelin. 2019. Dissolved inorganic nutrients including 5 macro nutrients: silicate, phosphate, nitrate, nitrite, and ammonium from water column bottle samples collected between October and April at Palmer Station, 1991 - 2019. ver 9. Environmental Data Initiative. https://doi.org/10.6073/pasta/8f9b7a10633d6eed2e8c0f2eefb8ac0c (Accessed 2022-11-16).

Parra, R. R. T., Laurido, A. L. C. & Sánchez, J. D. I. Hydrographic conditions during two austral summer situations (2015 and 2017) in the Gerlache and Bismarck straits, northern Antarctic Peninsula. *Deep Res. Part I* **161**, 103278 (2020). https://doi.org/10.1016/j.dsr.2020.103278.

Pitman, R.L., Durban, J.W. Killer whale predation on penguins in Antarctica. Polar Biol 33, 1589–1594 (2010). https://doi.org/10.1007/s00300-010-0853-5.

Plum, C., Hillebrand, H. & Moorthi, S. Krill vs salps: dominance shift from krill to salps is associated with higher dissolved N:P ratios. Sci Rep 10, 5911 (2020). https://doi.org/10.1038/s41598-020-62829-8.

Prézelin, B. B. et al. Physical forcing of phytoplankton community structure and primary production in continental shelf waters of the Western Antarctic Peninsula. J. Mar. Res., 62 (2004), pp. 419-460. https://doi.org/10.1357/0022240041446173

Prézelin, B. B. et al. The linkage between upper circumpolar deep water (UCDW) and phytoplankton assemblages on the west Antarctic Peninsula continental shelf. J. Mar. Res. 58, 165–202 (2000). https://doi.org/10.1357/002224000321511133.

Ratnarajah, L. & Bowie, A. R. Nutrient cycling: are antarctic krill a previously overlooked source in the marine iron cycle? Curr. Biol. 26, R884–R887 (2016).

Saba, G. K., et al. (2014), Winter and spring controls on the summer food web of the coastal West Antarctic Peninsula, Nat. Commun., 5, 4318. https://doi.org/10.1038/ncomms5318.

Sangrà, P., Gordo, C., Hernández-Arencibia, M., Marrero-Díaz, A., Rodríguez-Santana, A., Stegner, A., & Pichon, T. (2011). The Bransfield current system. Deep-Sea Research Part I Oceanographic Research Papers, 58(4), 390–402. https://doi.org/10.1016/j.dsr.2011.01.011.

Sangrà, P., Stegner, A., Hernández-Arencibia, M., Marrero-Díaz, Á., Salinas, C., et al. (2017). The Bransfield gravity current. Deep Sea Research Part I: Oceanographic Research Papers, 119, 1–15. https://doi.org/10.1016/j.dsr.2016.11.003.

Santoso, A., Mcphaden, M. J. & Cai, W. The Defining Characteristics of ENSO extremes and the Strong 2015/2016 El Niño. Rev. Geophys. 55, 1079–1129 (2017). https://doi.org/10.1002/2017RG000560.

Savidge, D. K., & Amft, J. A. (2009). Circulation on the west Antarctic peninsula derived from 6 years of shipboard ADCP transects. Deep Sea Research Part I: Oceanographic Research Papers, 56(10), 1633–1655. https://doi.org/10.1016/j.dsr.2009.05.011.

Secchi, E. R. et al. Encounter rates and abundance of humpback whales (Megaptera novaeangliae) in Gerlache and Bransfield Straits, Antarctic Peninsula. J. Cetacean Res. Manag. 3, 107–111 (2011). https://doi.org/10.47536/jcrm.vi.312.

Shepherd, A. et al. Mass balance of the Antarctic ice sheet from 1992 to 2017. Nature 558, 219–226 (2018). https://doi.org/10.1038/s41586-018-0179-y.

Sherrell, R.M., Annett, A.L., Fitzsimmons, J.N., Roccanova, V.J., Meredith, M.P., 2018. A 'shallow bathtub ring' of local sedimentary iron input maintains the Palmer Deep biological hotspot on the West Antarctic Peninsula shelf. Philos. Trans. R. Soc. A- Math. Phys. Eng. Sci. 376.

Silva, A. B.et al. 2020. Spatial and temporal analysis of changes in the glaciers of the Antarctic Peninsula. Glob. Planet. Chang. 2020, 184, 103079. https://doi.org/10.1016/j.gloplacha.2019.103079.

Stammerjohn, S. E., Martinson, D. G., Smith, R. C., Yuan, X. & Rind, D. Trends in Antarctic annual sea ice retreat and advance and their relation to El Ninño-Southern Oscillation and Southern Annular Mode variability. J. Geophys. Res. 113, C03S90 (2008). https://doi.org/10.1029/2007JC004269.

Su Z, Zhang Z, Zhu Y and Zhou M (2022) Long-Term Warm–Cold Phase Shifts in the Gerlache Strait, Western Antarctic Peninsula. Front. Mar. Sci. 9:877043. https://doi.org/10.3389/fmars.2022.877043.

Thompson, A. F. et al. Surface circulation at the tip of the Antarctic Peninsula from drifters. Journal Physics in Oceanographic, 39 (2009), pp. 3-26, https://doi.org/10.1175/2008JPO3995.1.

Tovar-Sanchez, A. et al. (2007). Krill as a central node for iron cycling in the Southern Ocean. Geophys. Res. Lett. 34:L11601. https://doi.org/10.1029/2006GL029096.

Turner, J., Guarino, M. V., Arnatt, J., Jena, B., Marshall, G. J., Phillips, T., et al. (2020). Recent decrease of summer sea ice in the Weddell Sea, Antarctica. Geophysical Research Letters, 47, e2020GL087127. https://doi.org/10.1029/2020GL087127.

Van Caspel, M., Hellmer, H.H., Mata, M.M. On the ventilation of Bransfield Strait deep basins. Deep Sea Res. Part II Top. Stud. Oceanogr., 149 (2018), pp. 25-30. https://doi.org/10.1016/j.dsr2.2017.09.006.

van Leeuwe, M. A., and others. 2020. Annual patterns in phytoplankton phenology in Antarctic coastal waters explained by environmental drivers. Limnol. Oceanogr. 65: 1651– 1668. https://doi.org/10.1002/lno.11477.

Venables, H. J., Meredith, M. P. & Brearley, A. Modification of deep waters in Marguerite Bay, western Antarctic Peninsula, caused by topographic overflows. Deep Res. Part II Top. Stud. Oceanogr. 139, 9–17 (2017). https://doi.org/10.1016/j.dsr2.2016.09.005.

Vera, C. S. & Osman, M. Activity of the southern annular mode during 2015–2016 El Niño event and its impact on southern hemisphere climate anomalies. Int. J. Climatol., 38 (2018), pp. e1288-e1295. https://doi.org/10.1002/joc.5419.

Wang, B. et al. Meteoric water promotes phytoplankton carbon fixation and iron uptake off the eastern tip of the Antarctic Peninsula (eAP). Prog. Oceanogr. 185, 102347 (2020). https://doi.org/10.1016/j.pocean.2020.102347.

Wang, X., Moffat, C., Dinniman, M.S., Klinck, J. M., Sutherland, D. A. & Aguiar-González, B. 2022. Variability and dynamics of along-shore exchange on the West Antarctic Peninsula (WAP) continental shelf. J Geophys Res Oceans 127: e2021JC017645.

Whitehouse, M. J., Atkinson, A. & Rees, A. P. Close coupling between ammonium uptake by phytoplankton and excretion by Antarctic krill, Euphausia superba. Deep Sea Res. Part Oceanogr. Res. Pap. 58, 725–732 (2011).

Zhou, M., Niiler, P. P., & Hu, J. H. (2002). Surface currents in the Bransfield and Gerlache straits, Antarctica. Deep-Sea Research Part I Ocean- ographic Research Papers, 49(2), 267–280. https://doi.org/10.1016/S0967-0637(01)00062-0.

Zhou, M., Niiler, P. P., Zhu, Y., & Dorland, R. D. (2006). The western boundary current in the Bransfield Strait, Antarctica. Deep Sea Research Part I: Oceanographic Research Papers, 53(7), 1244–1252. https://doi.org/10.1016/j.dsr.2006.04.003.